2008-08-13

I. Thermodynamics and Magnetism of Cu2OCl2 II. Repairs to Microcalorimeter the "2"s are subscripts, and the second 2 is preceded by a lower case L, not a one

Thomas J. Parry
Brigham Young University - Provo

I. Thermodynamics and Magnetism of Cu_2OCl_2

II. Repairs to Microcalorimeter

by

Thomas Parry

A thesis submitted to the faculty of

Brigham Young University

in partial fulfillment of the requirements for the degree of

Master of Science

Department of Chemistry and Biochemistry

Brigham Young University

December 2008

BRIGHAM YOUNG UNIVERSITY

GRADUATE COMMITTEE APPROVAL

of a thesis submitted by

Thomas Parry

This thesis has been read by each member of the following graduate committee and by majority vote has been found to be satisfactory.

Date	Juliana Boerio-Goates, Chair
Date	Brian F. Woodfield
Date	Roger Harrison
Date	Branton Campbell

As chair of the candidate's graduate committee, I have read the thesis of Thomas Parry in its final form and have found that (1) its format, citations, and bibliographical style are consistent and acceptable and fulfill university and department style requirements; (2) its illustrative materials including figures, tables, and charts are in place; and (3) the final manuscript is satisfactory to the graduate committee and is ready for submission to the university library.

BRIGHAM YOUNG UNIVERSITY

Date	Juliana Boerio-Goates Chair, Graduate Committee

Accepted for the Department

Date	David V. Dearden Graduate Student Coordinator

Accepted for the College

Date	Thomas W. Sederberg College of Physical and Mathematical Sciences

ABSTRACT

I. Thermodynamics and Magnetism of Cu_2OCl_2

II. Repairs to Microcalorimeter

Thomas Parry

Department of Chemistry and Biochemistry

Master of Science

Adiabatic calorimetry provides accurate and precise specific heat (C_p) data. From this data, thermodynamic functions may be calculated. Cu_2OCl_2, melanothallite, became of interest as part of a study of a particular thermochemical cycle. The experimental specific heat data and the calculated thermodynamic functions are reported here. Free energies of formation, calculated from the thermodynamic functions, suggest the particular cycle of interest with this compound as an intermediate is not feasible; uncertainty as to the accuracy of CuO and $CuCl_2$ data used in the calculations indicate further study may be necessary. Upon collection of the specific heat data, an antiferromagnetic transition was observed at 70 K; this led to examination of the magnetic heat capacity and entropy of the transition in melanothallite. The entropy of the transition was estimated to be 18.1 % and 7.5 % of 2Rln2 by two methods.

A theoretical calculation using an Ising model produced a result of 39 %. This is consistently low when compared to the entropies of the antiferromagnetic transitions of CuO and $CuCl_2$. This suggests geometric frustration. This thesis reports the thermodynamic functions calculated from the specific heat; the examination of the magnetic entropy; and repairs to an adiabatic apparatus involved in the collection of this data.

ACKNOWLEDGEMENTS

My thanks to Dr. Juliana Boerio-Goates for being my advisor and committee chair. Her patience, assistance and encouragement have been greatly appreciated. Dr. Brian F. Woodfield, for advice and assistance in repairing the microcalorimeter. I thank Trenton Walker, Tyler Meldrum, and Rebecca Olsen for assistance in collecting data on copper oxychloride. I rely on the previous work of Brian Lang, from whose dissertation I have liberally quoted and borrowed figures. I am grateful to Karren Williamson for assistance creating several figures in the microcalorimeter chapter. I thank Brigham Young University, for creating and maintaining an atmosphere where spiritual and scientific growth is encouraged.

I would also like to thank my family for their support. Without them I would not have made it. Their enthusiasm for my studies encouraged me. I appreciate their help, financial and other wise. I am especially thankful for the assistance of my sister Melinda, without whose assistance I would not be here.

Table of Contents

Table of Figures

List of Tables

Introduction

Our interest in melanothallite, Cu_2OCl_2, began as part of a project to determine the feasibility of a thermochemical cycle for hydrogen production. We set out in our experiments to determine the entropy at 298 K, calculate the thermodynamics of formation and observe the stability of the material with increasing temperature. These data allow a better understanding of the behavior and utility of melanothallite under various temperatures.

Melanothallite, or copper oxychloride, has magnetic properties that are of interest. Studies of the material indicate a structure conducive to magnetic effects and ordering, but also with the potential for geometric frustration.[1] The lattice and magnetic structure of melanothallite show similarities to both CuO and $CuCl_2$. Particularly useful is a comparison between the properties of melanothallite and CuO and $CuCl_2$. Both cupric oxide and copper dichloride exhibit magnetic transitions.[2,3] Of interest from a thermodynamics perspective is the magnetic entropy of these transitions; both vary from the theoretical prediction, given by 2S+1 where S is the spin angular momentum.[2,4]

The study of magnetism of materials is an ongoing interest in our research group. Of use in understanding the fundamental magnetism of the sample is the entropy of a magnetic ordering transition. The specific heat (C_p) study allows us to identify the existence of a transition and then calculate the entropy and the other thermodynamic functions.

Our specific heat measurements of copper oxychloride produced data between 15 K and 320 K. The results indicate a transition at about 70 K, a result confirmed by Kawashima, *et al.*,[5] published after our measurements were made. We made several calculations of the magnetic entropy from the collected data using different lattice approximations, in order to compare the estimated magnetic entropy to theoretically predicted values of said entropy.

Data collected on two adiabatic calorimetric instruments using the same Cu_2OCl_2 sample gave significantly different results. This led to the need for new tests to check the performance of one of the instruments. We chose to measure the heat capacity of benzoic acid on one of the instruments to observe

the calorimeter's accuracy and precision. During the experiment it became necessary to make changes to the physical design of the calorimeter. The most critical of these changes had been previously proposed by an earlier student but never completed.

Numerous problems were encountered during these experiments including excessive scatter within a consecutive set of data points and irreproducibility in the heat capacity results obtained from different sets of experiments over the same temperature region. These problems have been shown to result from unintended physical contact of the thermometer/heater leads with other parts of the cryostat. The instrument, the shields and heaters, and the leads were adjusted to remove the contact and thus the problem. These adjustments led to tests of the instrument to determine reproducibility between daily data series, over the course of a sample, and eventually, from one sample to another. It has been determined that this current arrangement gives reproducible results, but additional measurements are being made to establish the accuracy of the instrument.

This thesis describes the measurement of the heat capacity of melanothallite, and the calculation of the thermodynamic functions and estimation of the magnetic entropy of the copper oxychloride. Also described herein are the repairs, changes, and tests of the microcalorimeter to ensure reproducibility and accuracy of the data.

References

1) Krivovichev, S.V; Filatov, S. K.; The cuprite-like framework of OCu_4 tetrahedra in the crystal structure of synthetic melanothallite, Cu_2OCl_2, and its negative thermal expansion. *The Canadian Mineralogist* **2002,** *40*, 1185-1190
2) Stout, J. W.; Chisholm, R. C.; Heat capacity and entropy of $CuCl_2$ and $CrCl_2$ from 11 to 300 K. Magnetic Ordering in Linear Chain Crystals. *J. Chem. Phys.* **1962,** *36*, 979-971
3) Junod, A.; Eckert, D.; Triscone, G.; Müller, J.; Reichardt, W.; A study of the magnetic transitions in CuO: specific heat (1-330 K), magnetic susceptibility and phonon density of states. *J. Phys.: Condens. Matter* **1989,** *1*, 8021-8034

4) Loram, J.W.; Mirza, K.A.; Joyce, C.P.; Osborne, A.J.; Specific-Heat Evidence for Quasi-1D Magnetic Order in CuO. *Europhys. Lett.* **1989,** *8,* 263–268

5) Kawashima, K.; Okabe, H.; Suzuki, K.; Kuroiwa, S; Akimitsu, J.; Sato, K.H.; Koda, A.; Kadono, R.; Antiferromagnetic ordering in Cu_2OCl_2 studied by the muon spin rotation/relaxation technique. *J. Phys.: Condens. Matter* **2007,** *19,* 145275/1–145275/5

Chapter 1: Melanothallite (Cu_2OCl_2) Thermodynamics

We were asked to conduct heat capacity studies on melanothallite by Dr. Michele Lewis of Argonne National Laboratory as part of their hydrogen production studies. Our end goal was to generate entropies and thermodynamic functions of Cu_2OCl_2 and its stability as a function of temperature. This knowledge would aid in determining the feasibility of the hydrogen production cycle. To that end, the sample was also studied by reaction and differential scanning calorimetry by Professors Manuel A.V. Ribeiro da Silva and Maria D.M.C. Ribeiro da Silva at the University of Porto, Portugal, whose data is also mentioned here. Our continued interest in oxides and magnetism gave further motivation for the study.

1.1 Introduction

1.1.1 Hydrogen Production Cycle

Techniques for the low-cost, high-efficient production of hydrogen gas are in great demand. The use of H_2 in fuel cells has been investigated for many years because of its potential as a clean fuel source. At least two general methods of producing H_2 gas have been described in literature. One general approach uses electrochemical cells while the other one involves thermochemical cycles where the net effect is to produce H_2 and O_2 from water.[1-4]

One proposed thermochemical cycle uses the decomposition of Cu_2OCl_2 in hydrogen production as part of co-generation with nuclear reactor waste energy.[5] This cycle, as illustrated below, involves the copper oxychloride as an intermediate, not a starting material or an end product.

Proposed Cycle:

1. $2Cu + 2HCl(g) \rightarrow 2CuCl + H_2(g)$

2. $Cu_2OCl_2 \rightarrow 2CuCl + O_2(g)$

3. $2CuCl_2 + H_2O(g) \rightarrow Cu_2OCl_2 + 2HCl(g)$

4. $4CuCl \rightarrow 2CuCl_2(a) + 2Cu$ (electrochemical)

One feature of interest in this cycle is its lower operating temperature. The highest temperature in the cycle is between 450 and 530 ◦C.[5] The thermodynamic properties and functions of Cu_2OCl_2, a naturally-occuring mineral known as melanothallite, have not been explored beyond heat capacities and certain magnetic studies.[6] Structural studies have shown that melanothallite has the potential to lead to frustration in the magnetic arrangement.[7]

1.1.2 Data

We obtained third-law entropies and thermophysical functions from adiabatic calorimetric measurements of the crystalline heat capacity from 15 to 327 K. The enthalpy of formation was derived from solution calorimetric measurements performed elsewhere. The formation enthalpy has been combined with the third-law entropy of Cu_2OCl_2 and the entropies of the elements to generate the free energy of formation at 298.15 K. The heat capacity of Cu_2OCl_2 was found to be well represented by the sum of the heat capacities of CuO and $CuCl_2$ between 130 K and 320 K. The heat capacity sum was used to estimate the high temperature heat capacity of the oxychloride; the estimated heat capacity was then used to obtain high temperature thermodynamic functions.

Calculations of the free energy of formation suggest that as the free energy changes with temperature, the free energy of the reaction increases as temperature increases.

1.2 Experimental

1.2.1 Sample Preparation– Griffith University

The Cu_2OCl_2 sample was prepared and characterized by Professor Greg Hope at Griffith University (School of Biomolecular and Physical Sciences, Nathan campus, Griffith University, 170 Kessels Road, Nathan, QLD 4111, Australia) from stoichiometric amounts of CuO and $CuCl_2$ (Aldrich Chemical Co.) The starting materials were found to have a metals purity of > 99.995% and > 99.999% purity, respectively. Impurities found in the CuO include: Fe (12.8 ppm), Pt (8.4 ppm), and other metals in amounts < 1 ppm. The $CuCl_2$ contained impurities of Tl (6.00 ppm), Na (2.52 ppm), Ca (1.82 ppm), As (1.40 ppm), and Fe (1.21 ppm).

The sample was further characterized by gravimetric analysis. An amount of sample was dissolved in 5% HNO_3 solution; additional 5% HNO_3 solution was added to obtain a total volume of 100 mL. This solution was then analyzed for Cl^- as AgCl. From the 2.0149g dissolved sample, 0.2699 g AgCl was expected. Three measurements resulted in: 0.2705 g, 0.2673 g, and 0.2679 g. The X-ray diffraction (XRD) pattern performed and reported at Griffith University confirmed the sample to be single phase melanothallite.

1.2.2 Adiabatic calorimetry – Brigham Young University

The heat capacity of Cu_2OCl_2 was measured in two cryostats: a small-sample adiabatic cryostat from 14 K to 320 K and in a large-sample adiabatic cryostat from 155 K to 320 K. The two instruments operate on essentially identical principles; only size and certain details of arrangement differ. Figures 1.1 and 1.2 show the large- and small-sample calorimeters, respectively.[8] Normal procedure only involves running the data collection on one instrument. Concern about accuracy caused the sample to be run in both apparatuses.

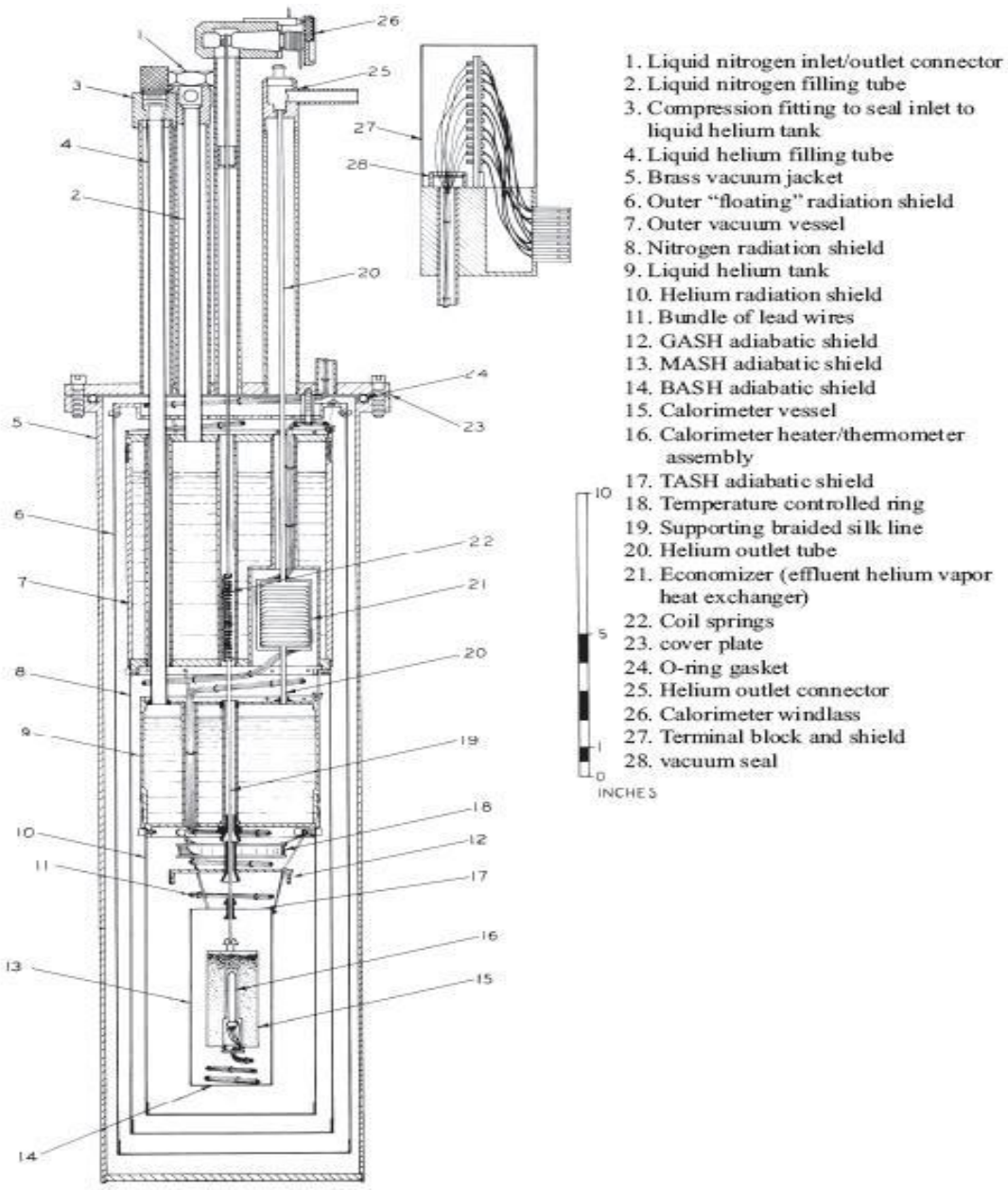

Figure 1.1: Schematic of large-sample calorimeter[8]

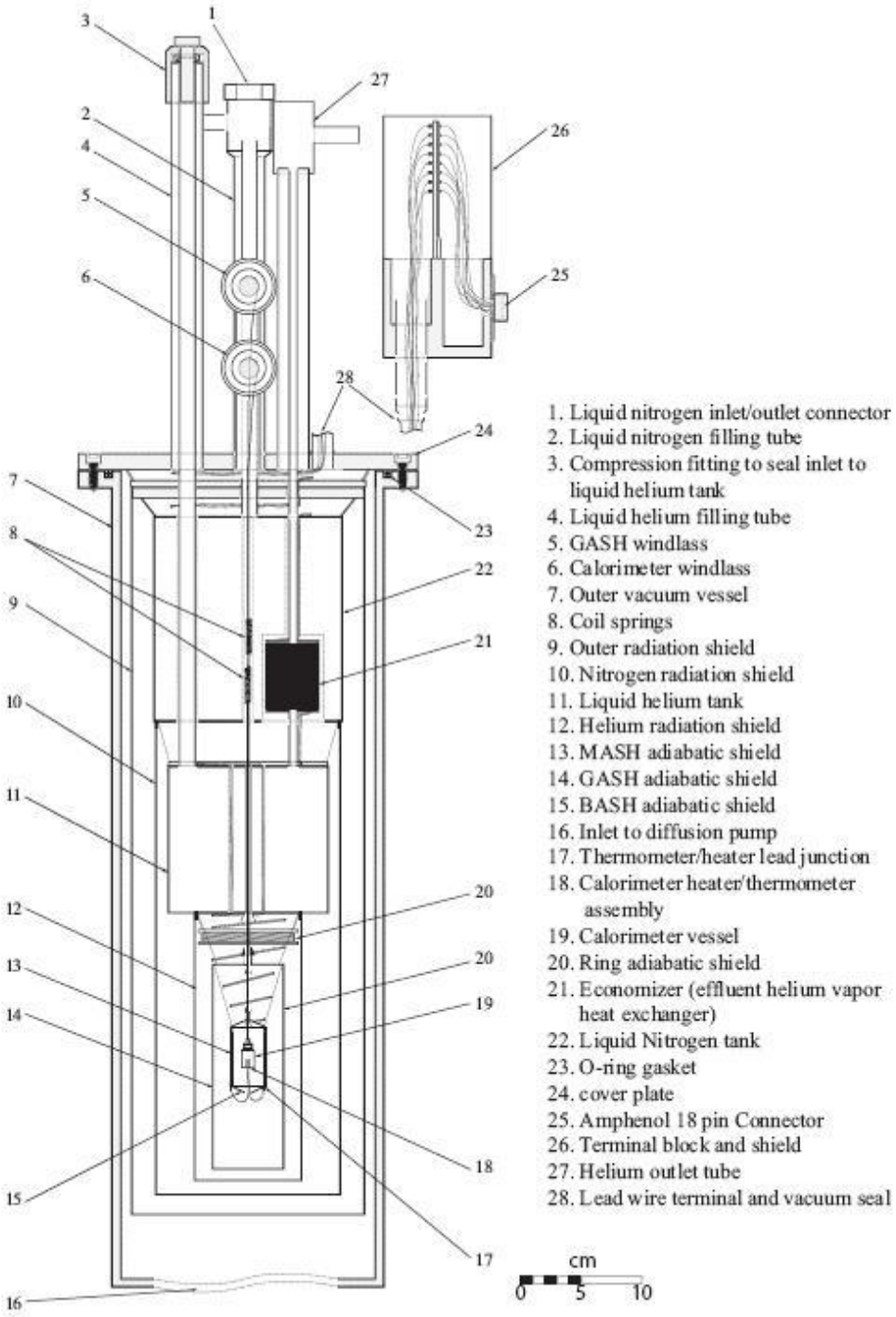

Figure 1.2: Small-sample calorimeter

The calorimeter in the small-sample unit has an internal volume of 0.875 cm^3. The apparatus incorporates adiabatic shield heaters whose temperatures are controlled via Proportional, Integral, and Derivative (PID) algorithms and a LABVIEW© interface board.[8] Temperatures are determined by measurement of the resistance of a platinum resistance thermometer using a Linear Research Inc. Model LR-700 AC Resistance Bridge. The temperature scale is that of the ITS-90.[8]

The smaller sample volume of this unit can be expected to lead to a reduced absolute accuracy compared to the large calorimeter results. However, two samples run earlier on this cryostat, CoO and Cu, gave results that were in good agreement with those reported in the literature. A third sample, β-FeOOH, gave results that were reasonable compared to other FeOOH polymorphs. Details of the construction, operation and performance tests of the small sample apparatus are described elsewhere.[8]

The large-sample calorimeter (10.5 cm^3 internal volume) is also described elsewhere.[9] Numerous compounds have been measured in this apparatus and its performance is well-documented.[9-12]

The copper oxychloride sample was received from Professor Greg Hope at Griffith University. Due to the possible decomposition of Cu_2OCl_2 in a moist atmosphere,[7] the sample was stored in an Ar-filled atmosphere in a glove box until the calorimetric experiments were begun. Water and O_2 levels remained consistently less than 5 ppm in this glove box.

Approximately 2.8 grams of sample were pelletized in the glove box and loaded first into the 10-cm^3 calorimetric vessel for the large-sample adiabatic calorimeter. The heat capacity was measured from 155 to 320 K in this cryostat. Over this temperature range, the contribution of the sample heat capacity was found to be less than 20% of the total measured heat capacity, and there was more scatter in the results than typically observed with this cryostat. We decided to transfer the sample to the small scale calorimeter and complete the measurements in that apparatus.

All manipulations on the copper oxychloride sample for the transfer to the small cryostat were again performed in the glove box. Heat capacities from this smaller-calorimeter cryostat yielded results in the range 15 to 320 K, in which the sample constituted around 45 – 56 percent of the total measured values. While this represented a large improvement over the results from the large-sample cryostat, the agreement

of the two sets of C_ps, as discussed below, became increasingly poor with increased T. I shall detail later evidence that this deviation arises from previously unknown heat leaks.

1.2.3 Reaction Calorimetry – University of Porto

The standard enthalpy of formation, $\Delta_f H°$, of Cu_2OCl_2 was measured via two independent sets of solution calorimetry experiments. One experimental cycle was based on the measurement of the enthalpies of solution of $CuCl_2$ (cr) and Cu_2OCl_2 (cr) in 0.1 mol/dm^3 HCl. The other experimental cycle involved measurements of enthalpies of solution of CuO (cr) and Cu_2OCl_2 (cr) in 4.0 mol/dm^3 HCl.

1.2.4 Differential Scanning Calorimetry – University of Porto

High temperature calorimetry to obtain the heat capacity (311 to 690 K) of Cu_2OCl_2 was performed at the University of Porto with a SETARAM Differential Scanning Micro calorimeter (power compensated) mode DSC 141. The masses of sample were weighed on a Mettler-Toledo model UMX2 ultra-micro balance. Aluminum crucibles of volume 30 mm^3 from SETARAM were used. Heat flow calibration involved synthetic sapphire (NIST-RM 720); temperature calibration used the melting temperatures of In and Sn with the same temperature ramp as would be used on the sample.

The ramp program stepped the temperature up at 20 K increments; the temperature scan rate was 2 K/min. The experimenters ran five different independent temperature scans (runs) and averaged the results. This included a blank run and a run with sapphire for each sample. The mass of Cu_2OCl_2 used for each run was approximately 85 mg.

The decomposition of Cu_2OCl_2 at 725 K limited the range of the DSC experiments to an upper limit of 690. Within this interval, 311 to 690 K, no other heat effect was detected. However, the C_p results disagreed significantly with the adiabatic calorimetry and the sum of $C_p(CuO) + C_p(CuCl_2)$. An attempt to collect DSC data on this sample at Brigham Young University failed when the copper oxychloride reacted with the aluminum crucible. We suspect that the discrepancy of the Porto DSC results compared to the adiabatic calorimetric results is due to a reaction of this nature.

1.3 Results

1.3.1 Heat Capacity Measurements

The (sample plus calorimeter) heat capacities obtained on the large sample cryostat from 155 to 320 K showed the typical precision about a smooth curve that we normally obtain on this instrument. However, subtraction of the large empty calorimeter contribution and multiplication by the large molar factor arising from the small sample mass gave molar heat capacities that displayed a higher than normal degree of scatter; 2% versus 0.1%. For this reason we performed measurements with the small sample cryostat (14 to 320 K) where a smaller subtraction led to a scatter of about 0.5% around the smoothed curve in the region of overlap. Table 1 lists the data obtained from the small calorimeter while Table 2 lists the data from the large sample calorimeter and the results from both apparatuses are plotted in Figure 1.3. (Note: Tables are found at the end of this chapter.)

As can be seen in Figure 1.3, the results from the two adiabatic calorimeters diverge above 206 K. To calculate the thermodynamic functions from the heat capacity, we chose to discard the values above 206 K from the small-sample calorimeter. This choice was based on the observation that the values from the large calorimeter agree better with the sum of the heat capacities of CuO and $CuCl_2$ in this region. In fitting smoothed curves to the experimental results, we used a combined data set consisting of the values from the small calorimeter below 206 K and the data from the large unit above that temperature. The circles represent the data from the small calorimeter, and the squares the data from the large calorimeter. The diamonds represent the sum of CuO and $CuCl_2$ heat capacities from the literature.[13,14] The solid line represents a Debye-Einstein fit of the data according to Equation 1, and the fit parameters are listed in Table 3.

$$C_{p,m}(Cu2OCl2) = 3R\left[\frac{3n_D}{\left(\frac{\Theta_D}{T}\right)^3}\int_0^{\frac{\Theta_D}{T}}\frac{x^4\exp(x)}{(\exp(x)-1)^2}dx + n_E\left(\frac{\Theta_E}{T}\right)^2\frac{\exp\left(\frac{\Theta_E}{T}\right)}{\left(\exp\left(\frac{\Theta_E}{T}\right)-1\right)^2}\right]$$

Equation 1: Debye-Einstein fit equation

The inset to Figure 1.3 shows a close-up of the transition, with the best fit line drawn through the transition. The dashed line in the inset represents an estimation of the lattice heat capacity. This will be discussed more in the next chapter.

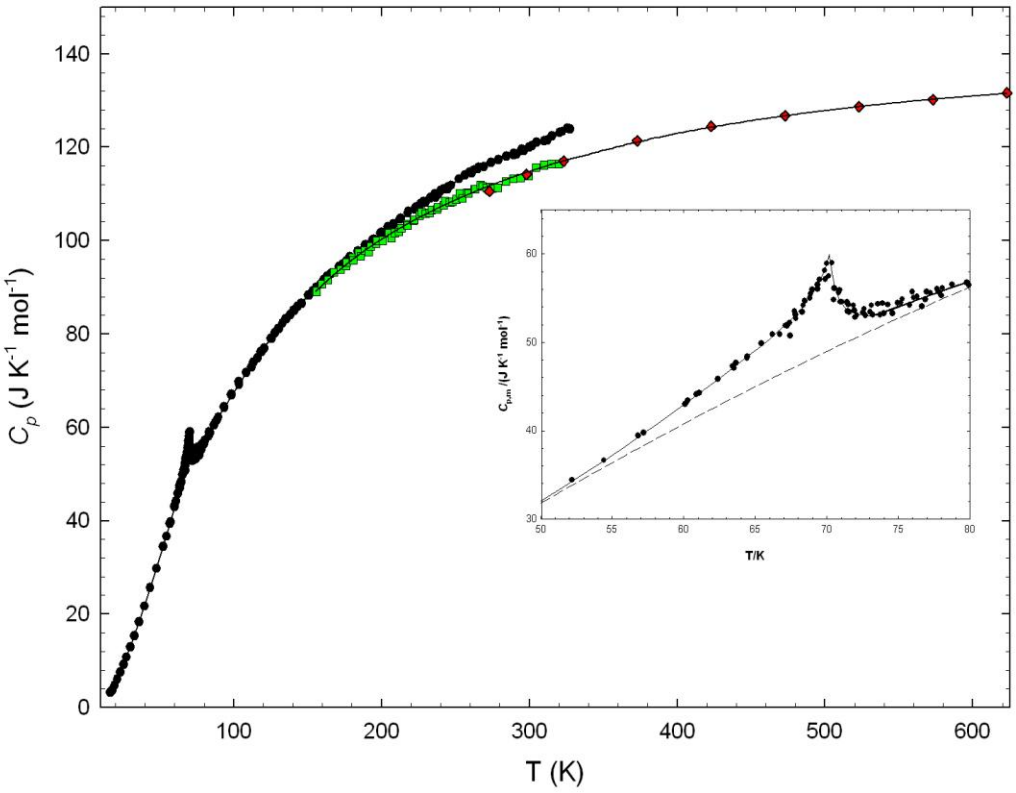

Figure 1.3: Melanothallite specific heat: Circles are data from microcalorimeter; squares are data from large calorimeter; diamonds are sum of CuO and $CuCl_2$ heat capacities from literature; line is Debye-Einstein fit and extrapolation of experimental data. **Inset:** Closeup of transition. Dashed line is estimation of lattice heat capacity (See Chapter 2)

The experimental results reveal the existence of a previously unknown phase transition in the Cu_2OCl_2. A peak appears in the plot of $C_{p,m}$ *vs T* with a maximum near 70 K (Figure 1.3 inset). The anomaly is a typical lambda-shaped peak with a slow increase of $C_{p,m}$ beginning at about 40 K, a maximum at 70.2 K, and a sharp decline down to about 73 K. However, the transition does not reproduce itself perfectly. A second, much smaller anomaly may also be present within the region from 73 to 74 K. This

second feature does not appear on every pass through this temperature region, nor does it appear at the same temperature, so we have not attempted to draw a curve to include it, but rather, we have drawn the heat capacity curve through a minimum near 72 K which is supported by more than half of the passes through this region (see Figure 1.3 inset).

Molar thermodynamic functions at a standard pressure of 1 bar, including the heat capacity, $C^{\circ}_{p,m}$, enthalpy increment, $H^{\circ}_{m}(T) - H^{\circ}_{m}(0K)$, entropy increments $S^{\circ}_{m}(T)-S^{\circ}_{m}(0K)$ and Gibbs energy increments, $\Phi = -(G^{\circ}_{m}(T) - H(0K))/T$ have been generated by fitting a series of orthogonal polynomials to the data in the non-transition regions and performing numerical integration within the transition region. Assuming that the crystal possesses no residual entropy, i.e., that $S(0K) = 0$, the entropy increment can be taken as the absolute standard molar entropy at temperature T, $S^{\circ}_{m}(T)$. These results are reported in Table 4.

1.3.2 Enthalpy of Formation Results

The solution calorimetry experiments at the University of Porto produced two results for the value of the enthalpy of formation of Cu_2OCl_2 (cr). The first cycle, in which enthalpies of solution of $CuCl_2$ and Cu_2OCl_2 were measured, resulted in a calculated $\Delta_f H$ at 298 K of –(384.2 +/- 2.2) kJ/mol. The second cycle, measuring the enthalpies of solution of CuO and Cu_2OCl_2, produced an enthalpy of –(379.2 +/- 2.7) kJ/mol or –(385.1 +/- 2.8) kJ/mol for the enthalpy of formation of Cu_2OCl_2 (cr) depending on the value used for the enthalpy of formation of CuO (cr). This discrepancy arose based on the source of the enthalpy of formation for CuO and $CuCl_2$. By combining certain reactions in the cycles, the difference between the enthalpies of formation of $CuCl_2$ (cr) and CuO (cr) was deduced to be -57.1 kJ/mol. The use of the enthalpy of formation value for CuO provided by Nunez, Pilcher and Skinner,[15] compares well to the value for the enthalpy of formation of CuO calculated by adding this difference to the value for $CuCl_2$ from Moscow State University (MSU) online tables found at www.chem.msu.su/rus/tsiv/Cu/print-$CuCl_2$_c.html, as were the data for CuO and Cu metal[16,17,18]. These tables were accessed with the assistance of the web translation of www.appliedlanguage.com. The value for CuO provided by the MSU tables results in a calculation for the difference between the formation enthalpies of $CuCl_2$ and CuO that is significantly different (5 kJ/mol) than was deduced from the experiment. For this reason, the experimenters at the

University of Porto chose the value of –(385.1 +/- 2.8) kJ/mol on the basis that it used the value for the enthalpy of formation of CuO provided by Nunez et al.[15] They then averaged that result with the result from the first cycle, -(384.2 +/- 2.2) kJ/mol to arrive at a value of the enthalpy of formation of Cu_2OCl_2 to be -384.7 kJ/mol.

1.3.3 Differential Scanning Calorimetry Results

Table 5 lists the resultant average C_p of the five DSC high temperature data collection runs, as well as the sigma for each data point and the linear and quadratic fit data. The linear fit of the data is:

$$Cp \,/\, (\mathrm{J} \,/\, \mathrm{K} \,/\, \mathrm{g}) = 9.68029\ \mathrm{E{-}05} \times (T \,/\, \mathrm{K}) + 4.69013\ \mathrm{E{-}01}$$

The quadratic fit equation of the data is:

$$Cp \,/\, (\mathrm{J} \,/\, \mathrm{K} \,/\, \mathrm{g}) = -9.54145\ \mathrm{E{-}08} \times (T \,/\, \mathrm{K})^2 + 1.92278\ \mathrm{E{-}04} \times (T \,/\, \mathrm{K}) + 4.46383\ \mathrm{E{-}01}$$

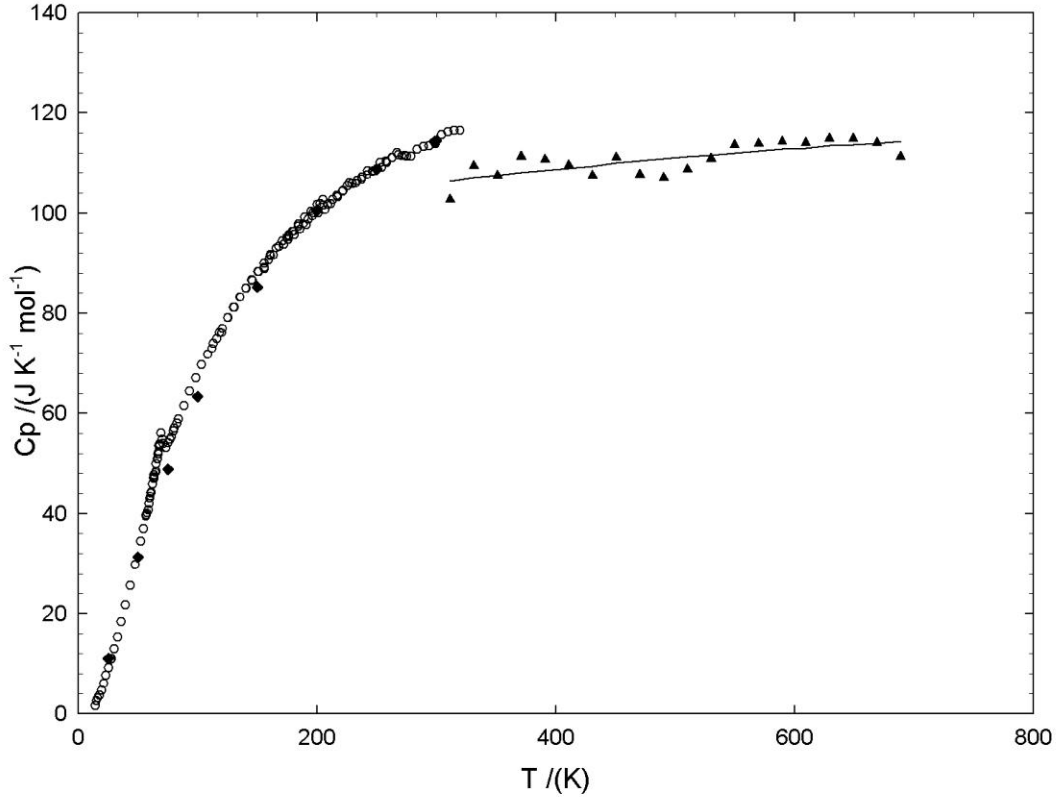

Figure 1.4: Comparison of Porto DSC data to adiabatic calorimeter data**:** Circles are experimental data, diamonds are the sum of the CuO and $CuCl_2$ specific heats; triangles are the University of Porto experimental data; line is linear fit of Porto data.

Figure 1.4 shows the plot of the DSC data from the University of Porto compared to our data. Both the linear fit and the data have been graphed. The quadratic data was not graphed, because it is indistinguishable from the linear fit on this graph. The data does not match well with ours; however, it should be noted that the DSC experimenters used aluminum crucibles. We attempted both a thermogravimetric analysis and DSC with the sample; the copper oxychloride apparently reacted with the aluminum crucibles we used.

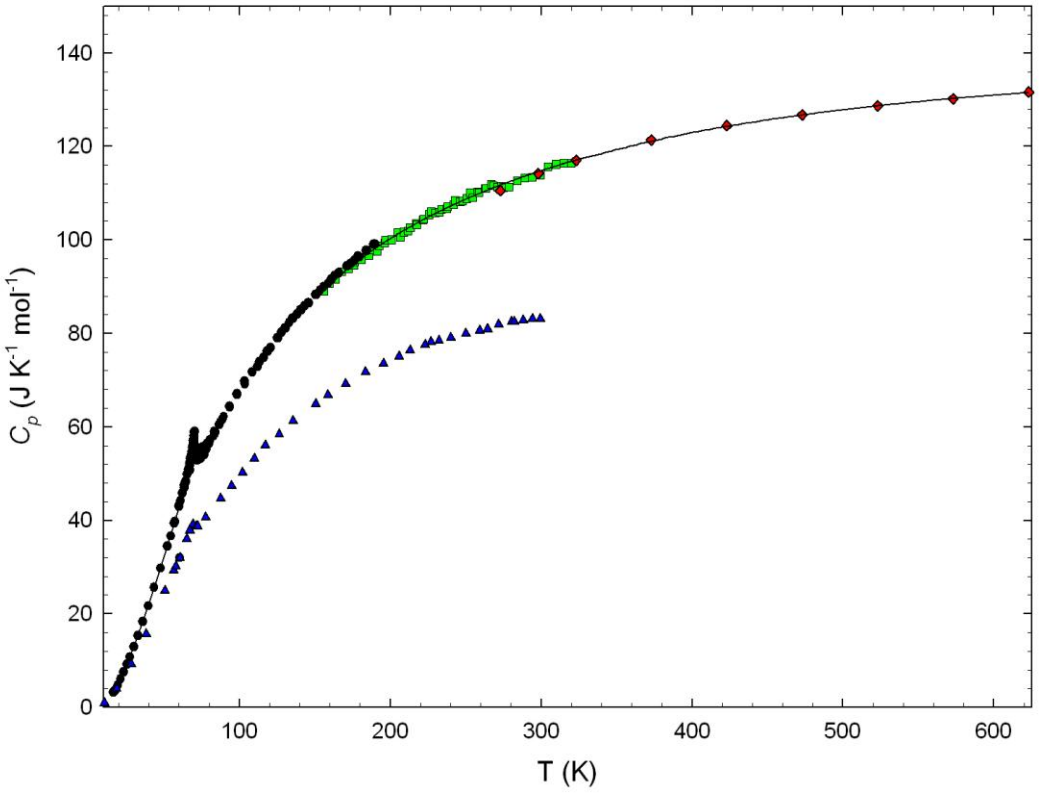

Figure 1.5: Experimental Cu_2OCl_2 data compared to Kawashima, et al.[6]

Circles are microcalorimeter data; squares are large calorimeter data; diamonds are sum of CuO and $CuCl_2$ literature data; triangles are data from Kawashima

1.4 Discussion

A recent study of melanothallite has produced heat capacity data of this compound by Kawashima, *et al.*.[6] However, comparison of their data to ours (Figure 1.5) shows their data to be significantly lower than ours. The data were scanned in from the article for the purpose of the comparison. It is possible that the apparatus used, a Physical Property Measurement System (PPMS), and poor sample thermal conductivity of the sample or a factor in its preparation may cause a difference in the scale of the data, as the transition does appear to be at approximately the same temperature, about 70 K.

1.4.1 Thermodynamic Functions

From the third law entropy and heat capacity functions, we calculated the thermodynamic functions of the copper oxychloride system. Thermodynamic functions of a substance include: the heat capacity C_p, the enthalpy increment, $H^\circ_m(T) - H^\circ_m(0K)$, entropy increments $S^\circ_m(T)-S^\circ_m(0K)$ and Gibbs energy increments, $\Phi = (G^\circ_m(T) – H(0K))/T$. These values then became useful in the examination of the thermochemical cycle, the primary purpose of studying melanothallite. These values are presented in Table 3. In order to determine the feasibility of the thermochemical cycle, several calculations were made: first, the high temperature free energy functions of the elements Cl_2, O_2, and Cu; second, the high-T enthalpy and free energy of the formation reaction of melanothallite; and finally the enthalpy and free energy of a formation reaction from CuO and $CuCl_2$.

The free energy calculations for the Cu_2OCl_2 suggest the copper oxychloride is more stable than the CuO and $CuCl_2$, even above the given decomposition temperature of 625K. The free energy increases as temperature increases, thereby decreasing the stability of the decomposition products. This result is not expected. Either copper oxychloride is more stable than the cupric oxide and the copper dichloride, or the calculation is in error. In the first case, this suggests that the cycle for hydrogen production being considered at Argonne National Laboratory is not suitable. In the second case, errors in the literature data, particularly the CuO data, should be a future focus of investigation.

References

1. Barbooti, M. M.; Al-ani, R. R.; The copper-chlorine thermochemical cycle of water splitting for hydrogen production *Thermochimica Acta* **1984,** *78,* 275-284
2. Kasahara, S.; Onuki, K.; Nomura, M.; Nakao, S; Static Analysis of the Thermochemical Hydrogen Production IS Process for Assessment of the Operation Parameters and the Chemical Properties *Journal of Chemical Engineering of Japan* **2006**, *39,* 559-568

3. Sakurai, M.; Miyake, N.; Tsutsumi, A.; Yoshida, K.; Analysis of a reaction mechanism in the UT-3 thermochemical hydrogen production cycle Int. J. Hydrogen Energy 1996 21 871-875
4. Fujii, K.; Ohkawa, K.; Hydrogen generation from aqueous water using n-GaN by photoassisted electrolysis *Phys. Stat. Sol.* **2006**, *3*, 2270-2273
5. Lewis, M; An assessment of the efficiency of the hybrid copper-chloride thermochemical cycle. 2005 annual meeting and fall showcase 05 AIChE; conference proceedings; Cincinnati, OH '05 Oct. 30-Nov. 4, 2005 348f/1-348f/3
6. Kawashima, K.; Okabe, H.; Suzuki, K.; Kuroiwa, S; Akimitsu, J.; Sato, K.H.; Koda, A.; Kadono, R.; Antiferromagnetic ordering in Cu_2OCl_2 studied by the muon spin rotation/relaxation technique. *J. Phys.: Condens. Matter* **2007,** *19*, 145275/1–145275/5
7. Krivovichev, S.V; Filatov, S. K.; The cuprite-like framework of OCu_4 tetrahedra in the crystal structure of synthetic melanothallite, Cu_2OCl_2, and its negative thermal expansion. *The Canadian Mineralogist* **2002,** *40*, 1185-1190
8. Lang, B. E.; Specific heat and thermodynamic properties of metallic systems : Instrumentation and analysis. Brigham Young Univ., Provo, UT, USA. Avail. UMI, Order No. DA3193054. (2005), 247 pp. From: Diss. Abstr. Int., B 2006, 66(10), 5423. Dissertation written in English. CAN 145:196721 AN 2006:771573 CAPLUS
9. Stevens, R; Boerio-Goates, J; Heat capacity of copper on the ITS-90 temperature scale using adiabatic calorimetry. *J. Chem. Thermodynamics*, **2004,** *36*, 857-863
10. Wang, L.; Vu, K.; Navrotsky, A.; Stevens, R.; Woodfield, B. F.; Boerio-Goates, J; Calorimetric study: surface energetics and the magnetic transition in nanocrystalline CoO. *Chem. Mater.*, **2004,** *16*, 5394-5400
11. Boyer, J. S.; Francis, M. R.; Boerio-Goates, J.; Heat-capacity measurements and thermodynamic functions of crystalline adenine; revised thermodynamic properties of aqueous adenine. *J. Chem. Thermodynamics* **2003,** *35*, 1917-1928
12. Donaldson, M. H.; Stevens, R.; Lang, B. E.; Boerio-Goates, J.; Woodfield, B. F.; Putnam, R. L.; Navrotsky, A.; Heat capacities and absolute entropies of UTi_2O_6 and $CeTi_2O_6$. *Journal of Thermal Analysis and Calorimetry* ***2005,*** *81*, 617-625

13. Hu, J-H; Johnston, H.L.; Low Temperature Heat Capacities of Inorganic Solids. XVI. Heat Capacity of Cupric Oxide from 15 to 300 ^{o}K. *J Am. Chem. Soc.* **1953,** *75,* 2471–2473
14. Stout, J. W.; Chisholm, R. C.; Heat capacity and entropy of CuCl2 and CrCl2 from 11 to 300 K. Magnetic Ordering in Linear Chain Crystals. *J. Chem. Phys.* **1962,** *36,* 979-971
15. Nunez, L.; Pilcher, G.; Skinner, H.A.; Hot-zone reaction calorimetry The enthalpies of formation of copper oxides. *J. Chem. Thermodynamics* **1969,** *1,* 31–43
16. Bergmann, G.A.; Gusarov, A.V.; Dichloride of Copper *translation of Moscow State University database website online at www.chem.msu.su/rus/tsiv/Cu/print-CuCl2_c.html through www.appliedlanguages.com* accessed 5-28-2008
17. Bergmann, G.A.; Gusarov, A.V.; Oxide of Copper *translation of Moscow State University database website online at www.chem.msu.su/rus/tsiv/Cu/print-CuO_c.html through www.appliedlanguages.com* accessed 5-28-2008
18. Bergmann, G.A.; Gusarov, A.V.; Copper *translation of Moscow State University database website online at www.chem.msu.su/rus/tsiv/Cu/print-Cu_c.html through www.appliedlanguages.com* accessed 5-28-2008

Tables

Table 1.1: Molar Heat Capacities of Cu_2OCl_2 Obtained from the Small Calorimeter

T/K	C_{pm}/(J·K^{-1}·mol^{-1})	T/K	C_{pm}/(J·K^{-1}·mol^{-1})	T/K	C_{pm}/(J·K^{-1}·mol^{-1})
14.278	1.661	71.506	54.239	145.517	86.591
15.213	2.63	71.555	53.417	146.02	86.504
16.45	3.191	71.861	54.177	150.628	88.319
17.779	3.694	71.945	53.582	151.127	88.275
19.44	4.746	71.977	52.816	153.467	89.171
21.32	6.016	72.088	53.066	155.745	89.949
23.34	7.578	72.214	51.62	158.593	90.609
25.517	9.181	72.503	54.406	160.862	91.63
27.393	10.751	72.548	53.325	160.949	91.417
27.862	10.99	72.605	53.758	163.281	92.383
29.974	12.913	72.69	53.042	166.075	92.957
32.877	15.337	72.902	51.226	171.207	94.404
36.069	18.318	73.019	53.413	173.543	94.871
39.584	21.673	73.127	54.158	174.32	95.065
43.444	25.595	73.189	53.129	176.348	95.587
47.662	29.75	73.227	53.073	178.689	96.473
52.199	34.43	73.459	54.718	179.474	96.296
52.398	34.326	73.558	54.32	183.833	97.745
54.408	36.618	73.735	53.105	184.624	97.752
56.806	39.446	73.909	54.39	188.979	99.06
56.846	39.406	73.986	53.248	189.767	99.119
57.186	39.741	74.264	54.239	194.133	100.166
59.529	41.971	74.498	56.007	194.915	100.334
60.085	42.99	74.611	53.268	199.276	101.608
60.204	43.226	74.942	54.442	200.069	101.701
60.291	43.419	75.186	54.496	202.211	101.585
60.876	44.097	75.278	54.888	202.739	101.808
61.08	44.231	75.783	54.188	204.42	102.933
62.38	45.823	75.973	55.727	205.227	102.659
63.397	47.284	76.072	55.059	207.383	103.257*
63.447	46.938	76.311	55.139	207.891	103.582*
63.503	47.067	76.89	54.828	212.549	104.617*
63.651	47.631	77.242	55.561	213.044	104.713*
64.422	48.185	77.701	56.027	217.707	105.946*
64.442	48.378	77.816	55.7	218.2	106.234*
65.432	49.864	78.018	55.286	222.577	106.627*
65.686	50.556	78.018	55.286	222.876	106.931*
66.2	50.885	78.092	56.145	223.361	107.196*
66.455	51.756	78.76	56.538	226.69	107.894*
66.974	52.484	79.783	56.729	228.037	108.033*
67.117	51.877	79.923	56.471	228.53	108.274*
67.228	51.841	80.348	57.087	229.794	108.226*
67.303	52.043	80.499	57.047	232.902	109.078*

T/K	C_{pm}/(J·K^{-1}·mol^{-1})	T/K	C_{pm}/(J·K^{-1}·mol^{-1})	T/K	C_{pm}/(J·K^{-1}·mol^{-1})
67.343	47.741	80.499	57.047	233.201	109.161*
67.382	52.191	80.619	57.222	236.013	109.951*
67.443	50.722	82.857	58.015	236.781	109.219*
67.737	53.496	83.373	58.962	238.36	109.954*
67.808	53.106	83.648	58.767	240.15	110.672*
67.846	52.671	83.774	58.463	241.944	111.006*
67.974	48.106	84.002	58.875	244.759	110.937*
68.252	53.406	86.666	60.504	245.325	111.413*
68.316	53.407	87.366	60.991	247.108	111.848*
68.355	54.155	88.467	61.446	252.278	113.190*
68.459	54.66	88.71	61.498	256.404	113.972*
68.47	54.651	89.69	62.189	259.513	114.672*
68.824	55.016	93.42	64.371	261.108	114.442*
68.875	55.492	93.665	64.224	262.625	115.123*
68.973	55.931	98.382	67.03	265.236	115.348*
69.128	53.906	98.644	66.882	265.738	115.725*
69.343	56.505	103.357	69.718	269.385	115.798*
69.352	56.018	103.634	69.18	274.041	116.761*
69.382	56.047	108.38	71.751	279.225	117.292*
69.463	53.732	108.642	71.64	284.412	118.054*
69.487	57.094	112.152	72.866	284.412	118.054*
69.79	55.624	113.397	73.921	289.41	118.358*
69.858	58.132	113.66	74.028	289.59	118.712*
69.886	57.112	116.023	74.881	289.59	118.712*
70	58.897	118.436	76.184	291.229	118.410*
70.133	57.478	118.709	76.145	294.6	119.215*
70.369	58.991	120.595	76.898	294.765	119.514*
70.412	56.734	125.165	79.053	294.765	119.514*
70.482	54.811	125.666	79.07	296.4	119.230*
70.483	54.417	128.006	80.22	299.782	120.030*
70.52	56.117	130.234	81.126	301.572	120.266*
70.825	55.584	130.739	81.148	304.961	121.065*
70.901	55.907	133.06	82.254	310.126	121.358*
70.942	54.576	135.317	83.198	311.939	121.434*
71.03	54.568	135.822	83.193	315.294	122.383*
71.167	52.002	138.137	84.11	320.497	123.134*
71.28	53.933	140.41	84.938	322.29	123.356*
71.416	54.549	140.913	84.987	325.685	124.022*
71.458	53.495	143.232	85.839	327.462	123.895*

* These data from the small calorimeter were not used because the data from the large calorimeter were felt to be more accurate above 206 K

Table 1.2 : Molar Heat Capacities of Cu_2OCl_2 Obtained from the Large Calorimeter

T/K	C_{pm}/(J·K^{-1}·mol^{-1})	T/K	C_{pm}/(J·K^{-1}·mol^{-1})
155.798	89.121	232.367	105.945
159.767	90.676	233.879	106.471
163.873	91.547	237.528	106.754
167.985	93.269	238.014	107.146
172.098	93.777	242.151	107.628
175.969	94.664	242.686	108.423
176.213	95.289	246.290	108.220
180.332	96.312	247.741	108.394
180.864	95.723	250.428	108.854
184.454	97.349	252.874	110.090
186.002	96.713	254.540	109.104
188.526	97.842	258.040	110.288
191.145	97.614	258.657	110.082
192.612	98.763	262.793	111.025
196.289	99.384	263.213	111.012
196.735	99.956	266.932	111.972
200.860	100.049	268.384	111.619
204.989	101.584	271.075	111.387
206.617	100.629	273.559	111.436
209.121	101.680	275.218	111.266
211.746	101.873	278.736	111.322
213.252	102.697	283.908	112.703
216.895	103.470	289.084	113.212
217.383	103.244	294.211	113.376
221.500	104.310	299.362	113.875
222.049	104.475	304.532	115.666
225.613	105.413	309.708	116.200
227.206	106.018	314.889	116.456
229.743	105.849	320.066	116.470

Table 1.3 : Parameters in Eq. 1 that represent $C_{p,m}(Cu_2OCl_2)$ from 298 to 625 K.

n_D	1_D/K	n_E	1_E/K
4.654	373.41	0.945	1193

Table 1.4 : Standard Molar Thermodynamic Functions of Cu_2OCl_2

T/K	C_{pm}/(J·K^{-1}·mol^{-1})	$H^\circ(T)-H^\circ(0)$/(kJ·mol^{-1})	$S^\circ(T)-S^\circ(0)$/(J·K^{-1}·mol^{-1})	Φ/ (J·K^{-1}·mol^{-1})
20	5.116	0.033	2.704	1.063
30	12.912	0.122	6.199	2.144
40	22.115	0.295	11.131	3.749
50	32.096	0.566	17.142	5.812
60	42.993	0.941	23.934	8.256
66	50.582	1.221	28.378	9.881
70	58.937	1.436	31.542	11.027
70.165	59.937	1.446	31.682	11.075
74	53.127	1.653	34.557	12.219
80	56.882	1.984	38.858	14.056
90	62.301	2.580	45.873	17.204
100	67.471	3.229	52.707	20.414
110	72.345	3.929	59.369	23.653
120	76.850	4.675	65.860	26.901
130	80.956	5.464	72.176	30.142
140	84.676	6.293	78.313	33.365
150	88.056	7.157	84.273	36.561
200	100.065	11.878	111.354	51.964
250	109.066	17.117	134.696	66.229
298.15	114.117	22.493	154.352	78.909
300	114.407	22.705	155.058	79.376

Table 1.5 : University of Porto DSC data

T_m / K	C_p / (J/ K / g)		Fitting	
	average	sigma	linear	Quadratic
311.55	0.480	0.020	0.499	0.497
331.36	0.511	0.015	0.501	0.500
351.22	0.502	0.020	0.503	0.502
371.08	0.520	0.026	0.505	0.505
390.95	0.517	0.031	0.507	0.507
410.83	0.512	0.035	0.509	0.509
430.70	0.502	0.039	0.511	0.511
450.58	0.519	0.054	0.513	0.514
470.45	0.503	0.053	0.515	0.516
490.35	0.500	0.052	0.516	0.518
510.21	0.508	0.049	0.518	0.520
530.10	0.518	0.046	0.520	0.521
549.98	0.531	0.043	0.522	0.523
569.87	0.532	0.034	0.524	0.525
589.73	0.534	0.032	0.526	0.527
609.62	0.533	0.033	0.528	0.528
629.50	0.537	0.034	0.530	0.530
649.38	0.537	0.033	0.532	0.531
669.26	0.533	0.035	0.534	0.532
689.14	0.520	0.035	0.536	0.534

Chapter 2: Magnetism of Cu_2OCl_2

2.1 Introduction

The magnetic transition of copper oxychloride, Cu_2OCl_2, otherwise known as melanothallite, at 70 K indicates interesting behavior tied to the structure of copper oxychloride. This mineral came to us as part of the above mentioned study of a particular hydrogen production cycle (Lewis *et al.*)[1] . Determining the thermodynamic properties of melanothallite for the purpose of establishing the efficiency of this cycle required determining the total entropy of the transition, as noted in chapter one. The magnetism of the copper oxychloride gave us another reason to study this material.

Studies have shown that the structure of melanothallite has the potential to lead to frustration in the magnetic arrangement (Krivovichev *et al.*)[2] . A given spin on an atom in a lattice interacts with its neighbors. The natural tendency, i.e. the lowest energy interaction, requires neighbors to have spins arranged to minimize the energy. In the case of antiferromagnetic ordering, this would be a condition where all the spins are opposed to their neighbors. Some arrangements lead to interactions with neighbors in multiple lattice directions that force the spin to violate the low energy requirement. This is geometric frustration. Antiferromagnetic geometric frustration causes the magnetic spin to be aligned the same direction as some of its neighbors. Our research group has previously studied other frustrated antiferromagnets.[3-8] Viewing the structure of melanothallite as distorted oxo-centered tetrahedra could explain magnetic frustration in that a spin on a given copper atom has two or three close neighboring Cu spins that frustrate the orientation for the given spin. The measured heat capacity curve shows a peak in the curve at about 70 K. This peak in the heat capacities results from a magnetic transition. Specific heat and magnetic studies confirm the presence of the transition.[9,10] This chapter discusses the third-law magnetic entropies calculated for this transition. These calculations were made from the adiabatic calorimetric measurements of the crystalline heat capacity as measured and reported from 15 to 320 K. This chapter also discusses the possibility that these results

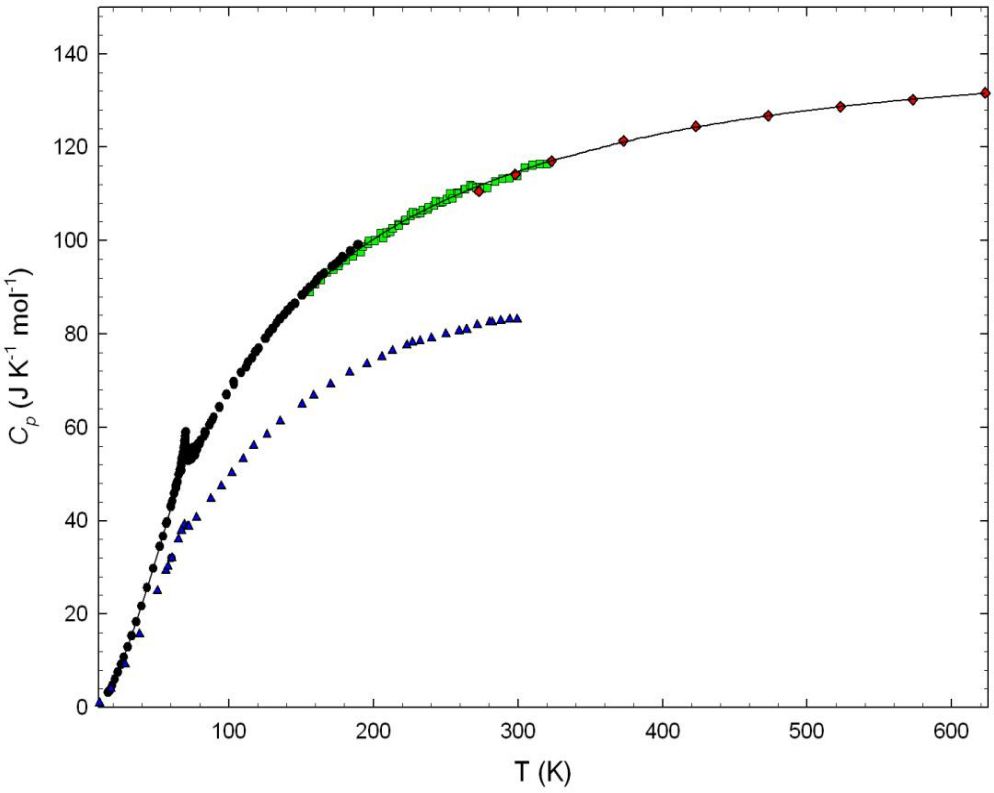

Figure 2.1: Experimental Cu_2OCl_2 data compared to Kawashima, et al.[10]

Circles are microcalorimeter data; squares are large calorimeter data;

diamonds are sum of CuOand CuCl2 data; line is Debye-Einstein fit;

triangles are Kawashima data

indicate for the influence of frustrated antiferromagnetism on the order in the lattice above the transition temperature.

2.2 Results

A recent heat capacity study of melanothallite has been reported by Kawashima, *et al,*.[4] as reported in Chapter 1. We again compare our C_p results to theirs for reference for this chapter; Figure 2.1 repeats the comparison of their data to ours from Chapter 1. This shows their data to be significantly lower than ours. Figure 2.1 also shows a comparison to the sum of the C_ps of CuO and $CuCl_2$. The relatively

good agreement of this sum with our data suggests that our data is accurate. As stated previously, it is possible that poor thermal conductivity of the sample or a factor in its preparation may cause a difference in the scale of the data, as the transition does appear to be at approximately the same temperature, about 70 K.

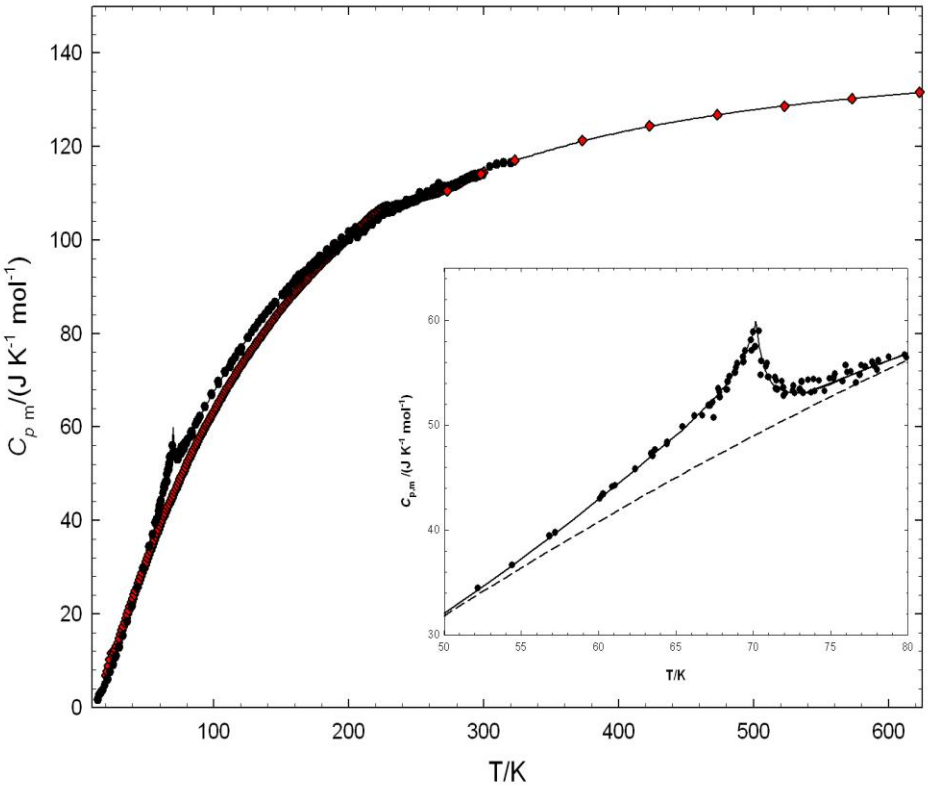

Figure 2.2: Melanothallite specific heat data. Circles are experimental data; Diamonds are the sum of CuO and $CuCl_2$ specific heats; Line is the Debye-Einstein fit of the experimental data. **Inset:** Circles are experimental data; line is Debye-Einstein fit; Dashed line is lattice heat capacity approximation from Debye-Θ method

Figures 2.1 and 2.2 show the measured C_p data and calculated fit data (solid line, also in Figure 2.2 inset) for Cu_2OCl_2 obtained from both adiabatic calorimeters (small=circles, large = squares). Also shown is the sum of CuO and $CuCl_2$ data (diamonds) calculated as an approximation of high-temperature behavior. The inset in Figure 2.2 shows a close-up of the transition, compared to an estimation of the lattice heat capacity (dashed line).

As described above, the calculation of entropy for the magnetic transition required approximations. The entropy of the transition is expected to approach $R\ln(2S+1)$ for each Cu atom in the formula; this results in an expected value of $2R\ln(2)$ for the magnetic entropy of the transition, since the spin, S, is 0.5 for copper. This upper limit allows a comparison between expected values and reasonable estimations to judge the extent of the transition.

2.2.1 Transition and its Entropy

The C_p peak at 70 K in Cu_2OCl_2 is due to a change in the magnetic order and magnetic structure in the lattice. As temperature decreases, the paramagnetic structure and disordered magnetic spins transition to a more ordered, antiferromagnetic structure. To extract a magnetic heat capacity and entropy from the measured sample C_p and entropy, it is necessary to determine a lattice heat capacity. The lattice heat capacity of a substance is the amount of energy absorbed by lattice vibrations in the sample before temperature increases.

The lattice heat capacity could not be estimated from the standard technique of interpolating from below the transition to high temperatures. This was difficult because of uncertainty as to the true starting and ending points of the transition. This uncertainty arises because the heat capacity is changing rapidly in this region, but the slope is beginning to decrease. This is a result of the increasing contribution of lattice vibrations nearing saturation as it approaches high temperatures. Two estimations of the lattice heat capacity were attempted. The first estimation simply involved taking the sum of CuO and $CuCl_2$ heat capacities; this sum has been shown to match well with the heat capacity of Cu_2OCl_2 at high temperatures (see Figure 2.1), and subtracting that sum from the measured copper oxychloride C_p. Data for CuO and $CuCl_2$ from Hu and Johnston[11], and Stout and Chisholm[12], respectively was used to calculate the sum. Cubic spline functions were fitted to the CuO and $CuCl_2$ data in a Mathcad program. These functions were then used to calculate C_ps at temperatures in the Cu_2OCl_2 dataset. The calculated C_p sum was then subtracted from the measured data to get an estimate of the magnetic heat capacity. Integration of the heat capacity as C_p/T resulted in the desired magnetic entropy. This entropy calculation produced a value 18.1 % of the expected $2R\ln(2)$.

The second method of estimation determined Debye theta values by inversion from the measured C_p values using a lookup table in a Mathcad file. The resulting Debye theta values were plotted by hand on graph paper. We estimated a set of Debye thetas by interpolation across the transition to approximate the lattice, as the more dramatic shape of the Debye theta curve allowed a better visual examination of where the transition began and ended. Figure 2.3 shows the plot of the Debye thetas versus T, with the

interpolation as the solid line. From this plot, a reasonable estimation of the lattice start and end points showed those to be about 39 and 84 K, respectively. The heat capacity was then calculated from this curve. This lattice heat capacity is plotted as the dashed line in the inset of Figure 2.1.

Comparison of the resultant lattice heat capacity to the data allowed a minor adjustment to

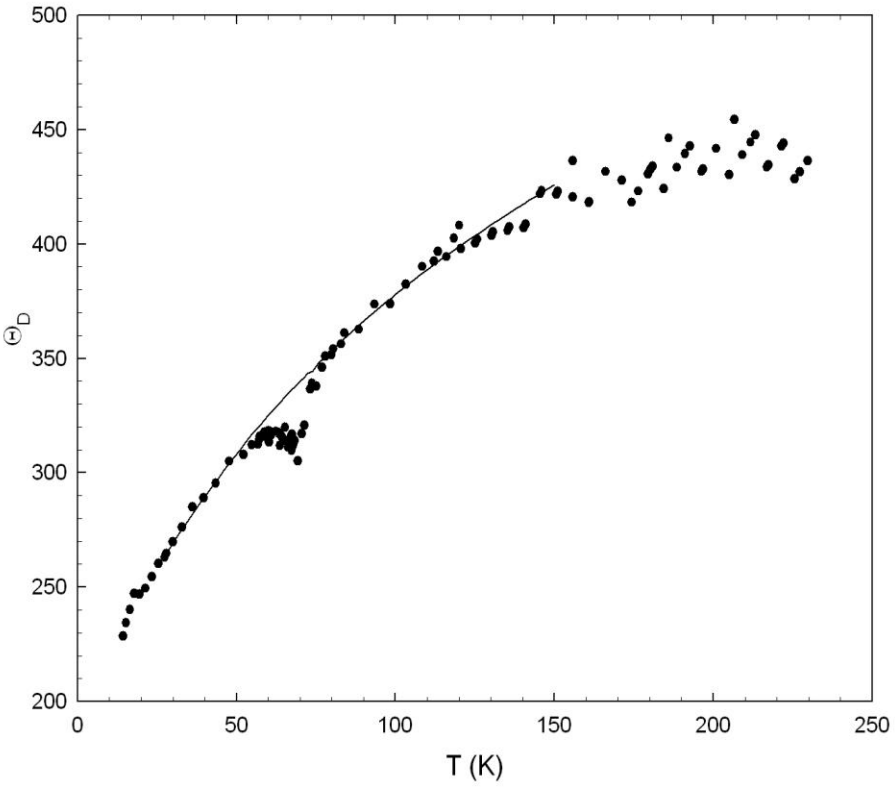

Figure 2.3: Debye-Theta vs T Line is hand-drawn curve used to estimate lattice specific heat.

produce better agreement with the experimental data at the high end. These data were compared to the transition. We used spline fits and interpolations in Mathcad to calculate the heat capacity excess above the estimated lattice heat capacity. We determined from this excess heat capacity the entropy to be 7.5 % of $2R\ln(2)$. The two magnetic heat capacities are shown in Figure 2.4.

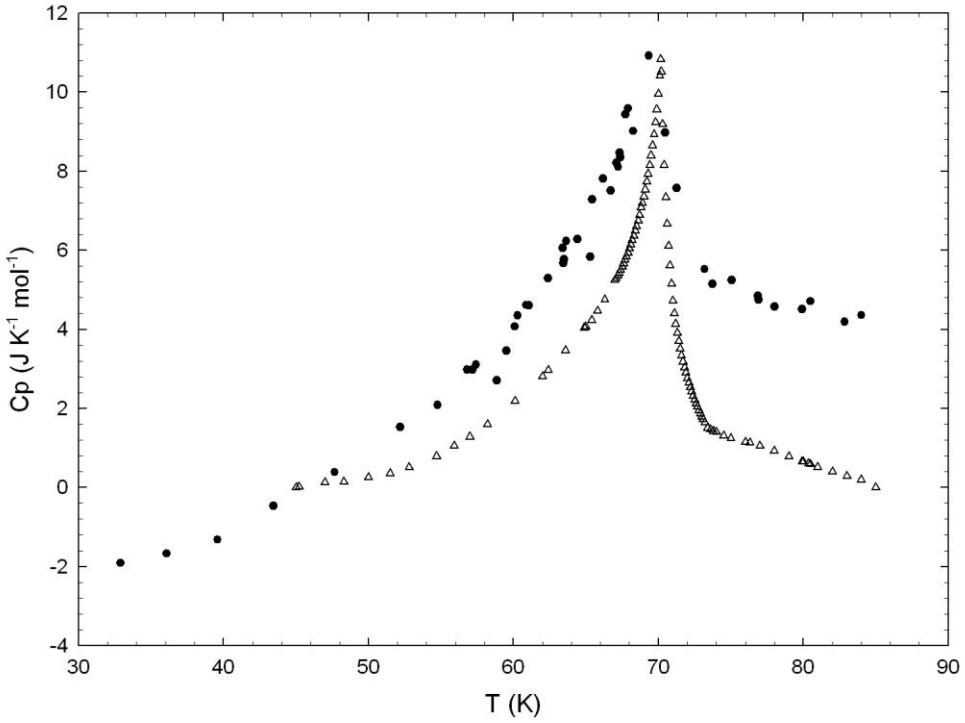

Figure 2.4: Estimated magnetic heat capacities. Circles are the magnetic heat capacities estimated from the sum of CuO and $CuCl_2$ data; Triangles are the estimated heat capacities from the Debye-Θ calculation.

2.3 Discussion

2.3.1 Crystal Structure of Melanothallite

The structure of copper oxychloride has been studied previously by Krivovichev, *et al.*[2] Their results indicate certain structural similarities to CuO and $CuCl_2$. Cu_2OCl_2 crystals have the orthorhombic Fddd structure and show negative thermal expansion along one axis of the unit cell.[2] Figure 2.5 shows the crystal structure of melanothallite, using the unit cell parameters reported by Krivovichev, *et al.*[2] This study suggests that the actual organization of the mineral could be considered as either chains of CuO_2Cl_2

squares organized into a linked framework (Figure 2.6) or as cuprite-like OCu_4 tetrahedra with Cl anions filling the voids[2] (Figure 2.7). The study by Kawashima, *et al.* of the magnetic properties indicates the presence of long-range order below 65 K and an antiferromagnetic transition at 70 K[1].

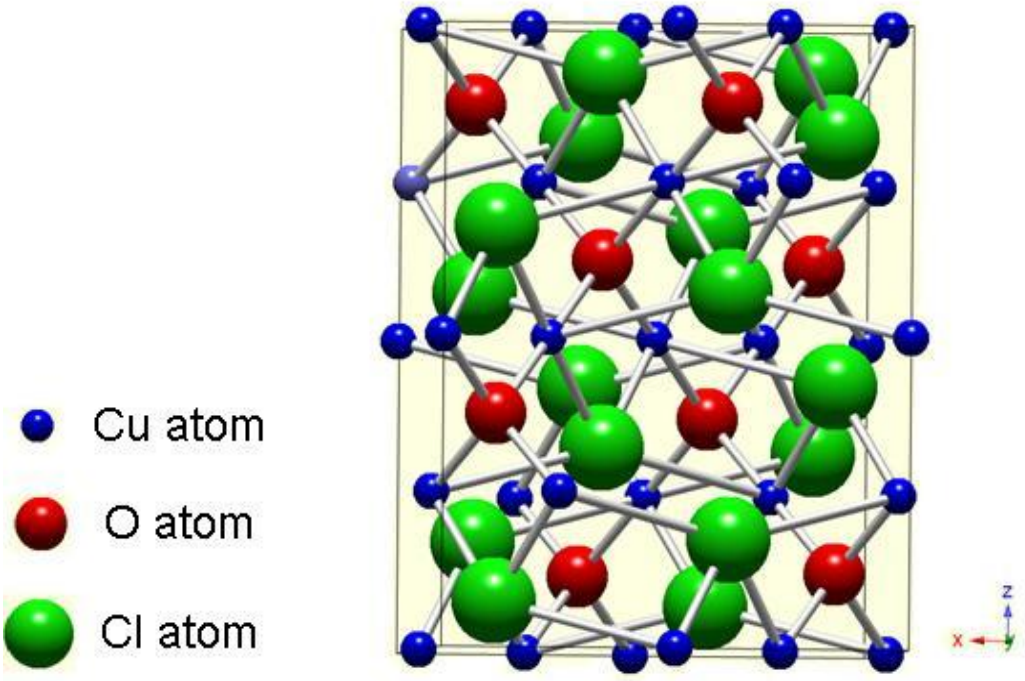

Figure 2.5: Crystal structure of Cu_2OCl_2

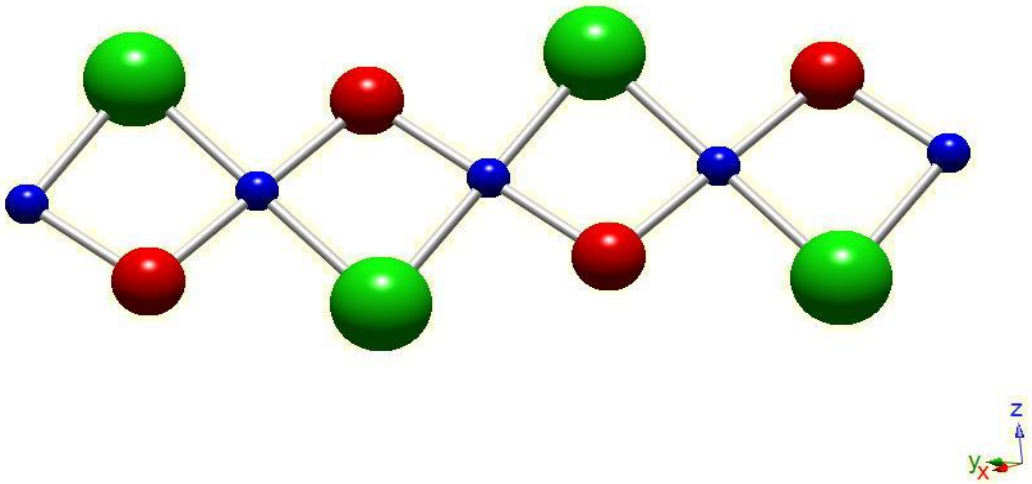

Figure 2.6: Chains of Cu^{2+} ions linked by O and Cl bridges

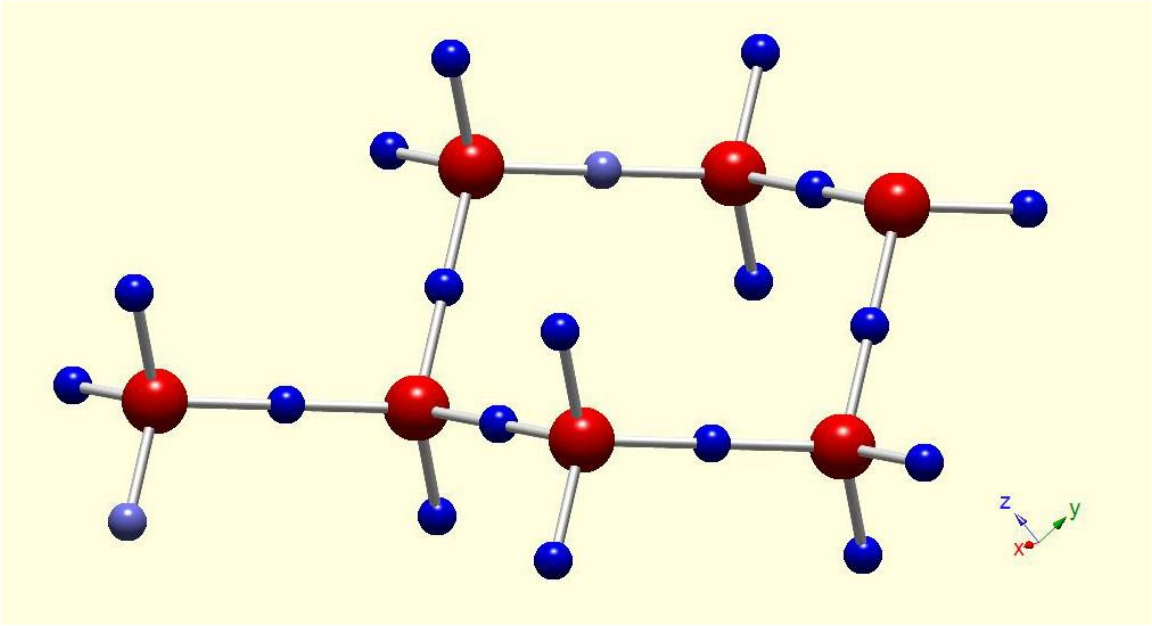

Figure 2.7: Distorted tetrahedra

The chains of edge-sharing CuO_2Cl_2 squares show similarities to the chain-like structure of $CuCl_2$. According to J. W. Stout and R. C. Chisholm,[12] $CuCl_2$ is organized as chains of copper ions surrounded by "four near chlorides" in parallel chains throughout the crystal (Figure 2.6), with two farther away chlorides from different chains "completing a distorted octahedron" (Figure 2.8). From studies of the heat capacity and the entropy of $CuCl_2$, these authors state that the metal ions interact strongly with neighboring Cl and O ions in the chain, while they interact weakly with Cl and O ions in neighboring chains. This leads to one-dimensional short-range order in the crystal, with the weaker interactions between chains possibly giving rise to long-range three-dimensional order at low temperatures.

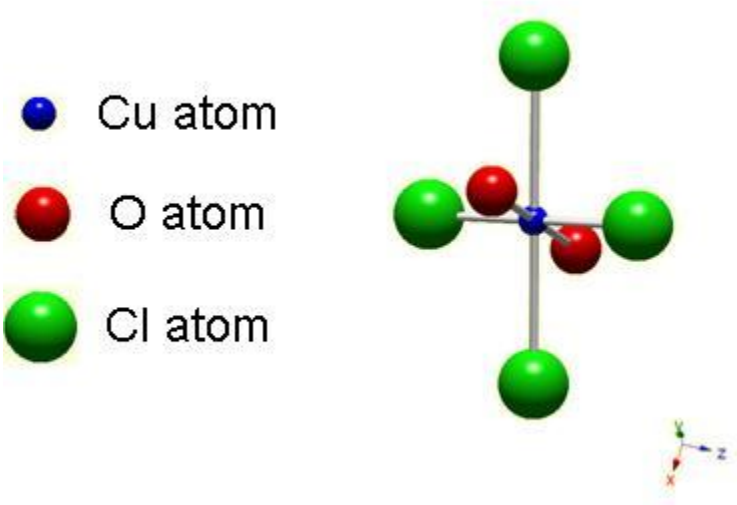

These results support the idea that the CuO_2Cl_2 squares and their chains

Figure 2.8: Distorted octahedron about an individual Cu^{2+} ion

interact antiferromagnetically to produce short-range, one-dimensional order. The strength and dimensionality of this order may differ from that of $CuCl_2$ because of the involvement of three types of atoms. However, the similarities in structural organization do evidence a qualitative similarity in order and dimensionality.

2.3.2 Comparison of Magnetic Structure of CuO and $CuCl_2$ to Cu_2OCl_2

CuO, having a square planar organization, also shows similarities to the structure of Cu_2OCl_2. This structure differs, however, in that the CuO contains interleaved sheets of CuO_2 of coordination of copper by oxygen, as opposed to the distorted octahedral coordination of $CuCl_2$ (Figure 2.8). Magnetically, the structure of CuO is more complicated than that of $CuCl_2$. Studies by Junod *et al.*[13] have shown that CuO has at least two magnetic transitions: a paramagnetic to incommensurate antiferromagnetic transition at 230 K as the substance is cooled, and an incommensurate antiferromagnetic to commensurate antiferromagnetic transition at 213 K with continued cooling. The incommensurate state has the antiferromagnetic ordering, whose unit cell does not match that of the atomic positions. The transition to the commensurate state "locks in" the ordering to correlate with the unit cell pattern. Estimation of the magnetic entropy at the transition at 230 K by Loram, *et al.*[14] to be approximately 29% of $R\ln(2)$ provides evidence of one-dimensional ordering in the lattice, and that the entropy increases even above the transition. The one-dimensional ordering reduces the entropy of the transition by preventing complete disorder in the lattice. A slower transition to complete disorder reduces the entropy change of the transition by spreading it out over a larger temperature range.

According to Stout and Chisholm,[12] $CuCl_2$ shows a magnetic transition at 23.9 K. Their calculations indicated that the magnetic entropy of that transition was approximately 27% of the expected $R\ln(2)$. Thus, magnetic entropy is still evolving above the peak transition temperature. The authors state that the transition at 23.9 K, as $CuCl_2$ is cooled, marks the beginning of 3-dimensional long-range ordering based on weak antiferromagnetic interactions between neighboring atoms in different chains. Above that temperature, short range antiferromagnetic ordering of nearest neighbors in the same chain occurs.

2.3.3 Magnetic Comparison of Ordering in Cu_2OCl_2 to CuO and $CuCl_2$

The magnetic transitions in CuO and $CuCl_2$ and the structural similarities indicate that the magnetic behavior of Cu_2OCl_2 could be described as a mixture of the effects. The higher temperature transitions in CuO, involving an incommensurate "intermediate" between the commensurate antiferromagnetic and paramagnetic states, involve one-dimensional order in the lattice and show that the entropy of transition does not approach the expected $R\ln(2)$. The entropy of the lower temperature transition of $CuCl_2$ also does not approach $R\ln(2)$, and suggests weak three-dimensional ordering. Taken together, the magnetic entropies of transition of CuO at 29 %[14] and $CuCl_2$ at 27 %[12] imply the existence of short range clusters.

These results, consistent with the low values of 18.1 % and 7.5 % obtained using both lattice models for copper oxychloride, also indicate that the magnetic transition may not be a complete transition, and that there may still exist short-range, clustered order in the lattice above the Néel temperature. The structure of the copper oxychloride suggests an explanation. If, as Krivovichev *et al.*[2] indicate, the structure of melanothallite can be represented as OCu_4 tetrahedra, the spins of the various copper atoms may not have the ability to freely arrange themselves relative to others. This is again similar to CuO, in that the structure of CuO can be interpreted as being two interpenetrating frameworks of OCu_4 tetrahedra.[2] In an antiferromagnetic state in these tetrahedra, not all the spins can orient themselves in directions opposite to those of every neighboring spin. This is the condition known as geometric antiferromagnetic frustration, an area of current research[15]. Figure 2.9 shows a simple example of geometric frustration. Each spin has two neighbors, and thus at least some of the spins cannot satisfy the minimization of energy by being opposed to all their nearest neighbors.

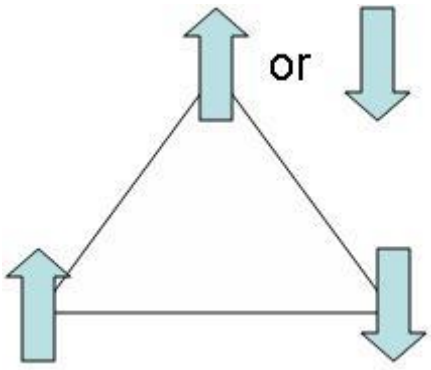

Figure 2.9: Simple example of geometric frustration

The chain-like structure of melanothallite serves as the foundation for another modeling possibility to attempt to examine the magnetic entropy. Mejdani and Lambros[16] theorize a ladder Ising spin model with inter- and intra-chain couplings as insight into spin chains. They developed a model equation

for the specific heat, with reduced temperature, ($k = J_{intra}/k_BT$) as the main variable and the two coupling constants, which we have chosen to call J_{intra} and J_{inter}. According to J-values suggested by Okabe, *et al.*[9], values of 112.6 K for J_{intra}, and 108 K for J_{inter}, were initially applied to the Ising model presented by Mejdani and Lambros.[16] Upon graphing of the specific heat calculated from the model, it was found that the data showed a maximum, but not at the temperature of the experimental data, 70 K. The coupling constants were then adjusted, moving the calculated peak to 70 K. The resultant values were: J_{intra} = 18 K, and J_{inter} = 99 K. According to Okabe, *et al.*,[9] As the ratio of J_{inter}/J_{intra} approaches 1, magnetic frustration and thereby 3-dimensional interaction would be enhanced. As the ratio approaches 0, intrachain and thereby low-dimensional magnetic interactions would dominate. These calculated results and the Okabe data[9] suggest that frustration and 3-dimensional order are present in melanothallite. Upon multiplication of the Ising ladder model calculated specific heat by $2R$ to get absolute temperatures, the magnetic entropy of the transition was calculated as 39 % of $2R\ln(2S+1)$. This result, though different from the other models, is still significantly smaller than the expected value.

The transition shows less a change in entropy than expected, because the spins do not become fully disordered immediately at the transition temperature. The structure is complicated by the presence of the chloride anions filling spaces. The results do suggest that the copper oxychloride generally shows short-range one-dimensional order, but that the transition is at a different temperature and has an apparently different and lower magnetic entropy of the transition because of interactions of three kinds of atoms instead of two. Such differing interactions may limit the ability of the melanothallite to become disordered to a greater extent than in CuO or $CuCl_2$. The Cu_2OCl_2 appears to have small clusters of locally ordered regions even at higher temperatures.

References

1. Lewis, M; An assessment of the efficiency of the hybrid copper-chloride thermochemical cycle. 2005 annual meeting and fall showcase 05 AIChE; conference proceedings; Cincinnati, OH '05 Oct. 30-Nov. 4, 2005 348f/1-348f/3

2. Krivovichev, S.V; Filatov, S. K.; The cuprite-like framework of OCu4 tetrahedra in the crystal structure of synthetic melanothallite, Cu_2OCl_2, and its negative thermal expansion. *The Canadian Mineralogist* **2002,** *40*, 1185-1190

3. Stevens, R.; Woodfield, B.F.; Boerio-Goates, J.; Crawford, M.K. Heat capacities, third-law entropies and thermodynamic functions of the geometrically frustrated antiferromagnetic spinels $GeCo_2O_4$ and $GeNi_2O_4$ from T = (0 to 400) K. *J Chem. Thermo.* **2004,** *36*, 359-375.

4. Lang, B. E.; Specific heat and thermodynamic properties of metallic systems : instrumentation and analysis. Brigham Young Univ., Provo, UT, USA. Avail. UMI, Order No. DA3193054. (2005), 247 pp. From: Diss. Abstr. Int., B 2006, 66(10), 5423. Dissertation written in English. CAN 145:196721 AN 2006:771573 CAPLUS

5. Stevens, R.; Boerio-Goates, J.; Heat capacity of copper on the ITS-90 temperature scale using adiabatic calorimetry. *J. Chem. Thermodynamics*, **2004,** *36*, 857-863

6. Wang, L.; Vu, K.; Navrotsky, A.; Stevens, R.; Woodfield, B. F.; Boerio-Goates, J.; Calorimetric study: surface energetics and the magnetic transition in nanocrystalline CoO. *Chem. Mater.*, **2004,** *16*, 5394-5400

7. Boyer, J. S.; Francis, M. R.; Boerio-Goates, J.; Heat-capacity measurements and thermodynamic functions of crystalline adenine; revised thermodynamic properties of aqueous adenine. *J. Chem. Thermodynamics* **2003,** *35*, 1917-1928

8. Donaldson, M. H.; Stevens, R.; Lang, B. E.; Boerio-Goates, J.; Woodfield, B. F.; Putnam, R. L.; Navrotsky, A.; Heat capacities and absolute entropies of UTi2O6 and CeTi2O6. *Journal of Thermal Analysis and Calorimetry* ***2005,*** *81*, 617-625

9. Okabe, H.; Suzuki, K.; Kawashima, K.; Muranaka, T.; Akimitsu, J.; New pyrochlore-like compound Cu_2OCl_2 with S = ½ *J Phys. Soc. Japan* **2006,** *75*, 123705-1-123705-4

10. Kawashima, K.; Okabe, H.; Suzuki, K.; Kuroiwa, S; Akimitsu, J.; Sato, K.H.; Koda, A.; Kadono, R.; Antiferromagnetic ordering in Cu_2OCl_2 studied by the muon spin rotation/relaxation technique. *J. Phys.: Condens. Matter* **2007,** *19*, 145275/1–145275/5

11. Hu, J-H; Johnston, H.L.; Low temperature heat capacities of inorganic solids. XVI. Heat capacity of Cupric Oxide from 15 to 300 ^{o}K. *J Am. Chem. Soc.* **1953,** *75*, 2471–2473

12. Stout, J. W.; Chisholm, R. C.; Heat capacity and entropy of CuCl2 and CrCl2 from 11 to 300 K. Magnetic ordering in linear chain crystals. *J. Chem. Phys.* **1962,** *36*, 979-971
13. Junod, A.; Eckert, D.; Triscone, G.; Müller, J.; Reichardt, W.; A study of the magnetic transitions in CuO: specific heat (1-330 K), magnetic susceptibility and phonon density of states. *J. Phys.: Condens. Matter* **1989,** *1*, 8021-8034
14. Loram, J.W.; Mirza, K.A.; Joyce, C.P.; Osborne, A.J.; Specific-heat evidence for quasi-1D magnetic order in CuO. *Europhys. Lett.* **1989,** *8*, 263–268
15. Singh, S.; Saha, S.; Dhar, S.K.; Suryanarayanan, R.; Sood, A.K.; Revcolevschi, A.; Manifestation of geometric frustration on magnetic and thermodynamic properties of the pyrochlores $Sm_2X_2O_7$(X=Ti,Zr) *Phys Rev B* **2008,** *77*, 054408-1-054408-7
16. Mejdani, R.; Lambros, A.; Ladder Ising spin configurations I. Heat capacity *Phys. Stat. Sol.* **1996,** *196*, 433-441

Chapter 3: The Microcalorimeter and its Reproducibility

3.1 An Overview of the Small Volume Calorimetric Apparatus and its Problems.

3.1.1 Melanothallite Inconsistency

As discussed in chapter 1, heat capacity measurements of melanothallite were made using two adiabatic calorimetric apparatuses, one a calorimeter with sample volume of 0.875 cm^3, hereafter referred to as the "microcalorimeter," and the other, having a volume of 10.5 cm^3, referred to as the "large calorimeter." An excessively large scatter was observed in the data obtained in the large calorimeter at higher temperatures $T > 170\ K$. The scatter was attributed to the small mass of sample and relatively large contribution of the empty calorimeter to the total measured heat capacity. It was expected that the smaller C_p of the microcalorimeter would improve the situation, so the sample was transferred to the microcalorimeter to finish the measurements (Figure 3.1).

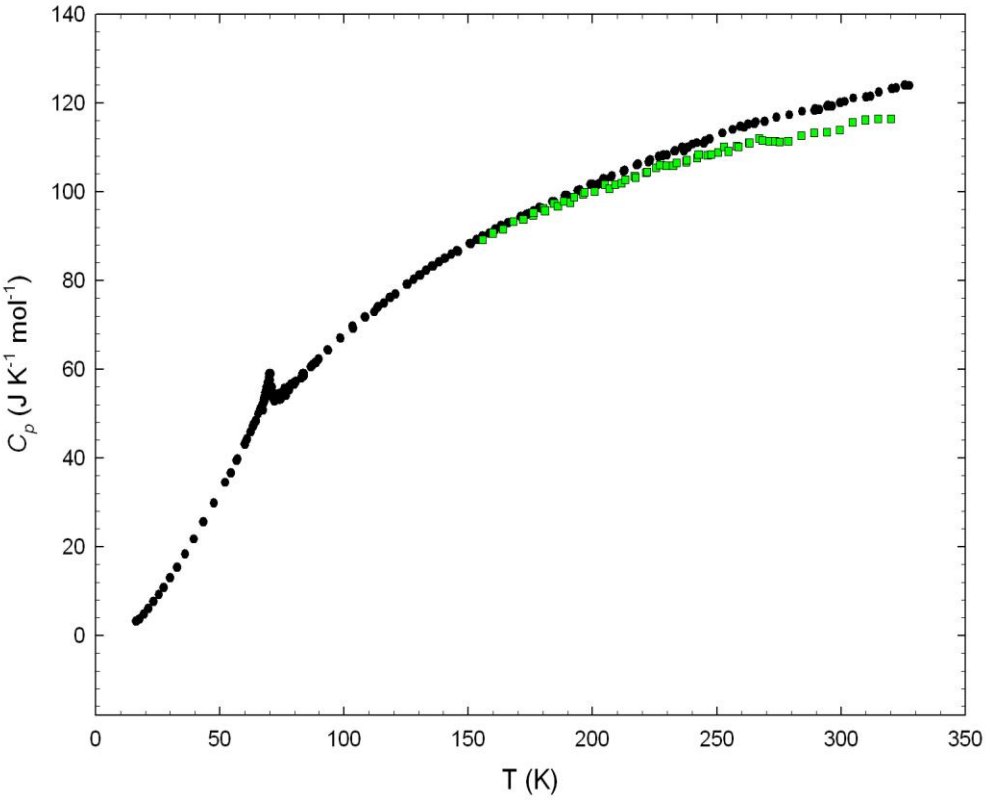

Figure 3.1: Cu_2OCl_2 specific heat data. Circles are microcalorimeter data; Squares are large calorimeter data

Unfortunately, the microcalorimeter experiments did not agree well with the earlier measurements at T > 180 K. The microcalorimeter C_p's were generally high. The data did, however, agree between 150 K and 180 K, so the data below about 150 K from the microcalorimeter was matched with the data from the large calorimeter, and thermodynamic calculations were performed on this combined dataset.

As discussed in chapter 1, the good agreement of the large calorimeter results with the sum (C_p(CuO) + C_p($CuCl_2$)) led us to suspect the problem lay with the microcalorimeter. The modifications to the calorimeter and its characterization have been reported in the Ph.D thesis of Brian Lang.[1] To explore the origins of the problem, the C_p of benzoic acid , a standard reference material[2,3], was measured. (NIST standard reference material 39i) Pellets totaling 0.52575 g of the calorimetric standard benzoic acid were loaded into the microcalorimeter.

The dissertation of Brian Lang discusses in great detail the design, operation and instrumentation of the microcalorimeter.[1] This thesis does not intend to investigate or thoroughly report the design and

function of the calorimeter. However, to facilitate discussion of the efforts that make up my thesis, sufficient description of the instrument will be made here to allow reference for the repairs. Where noted, a few diagrams have been reproduced from Lang's dissertation.[1]

3.1.2 Calorimetric Vessel

The microcalorimeter shares the same fundamental design principles as the large calorimeter, although the actual construction and operation involves certain key differences.[1,4] The term calorimeter technically refers only to the vessel that holds the sample and with which the thermometer/heater is intimately in contact. The term cryostat is the term for the entire instrument. The design ideally prevents contact of the thermometer/heater with any other surface. The reduction in scale requires certain design alterations, while collection and calculation of the data, though similar in execution, take advantage of different techniques (Figures 3.2 and 3.3). These design differences, while allowing for the use of smaller sample sizes, require altered handling and loading techniques.

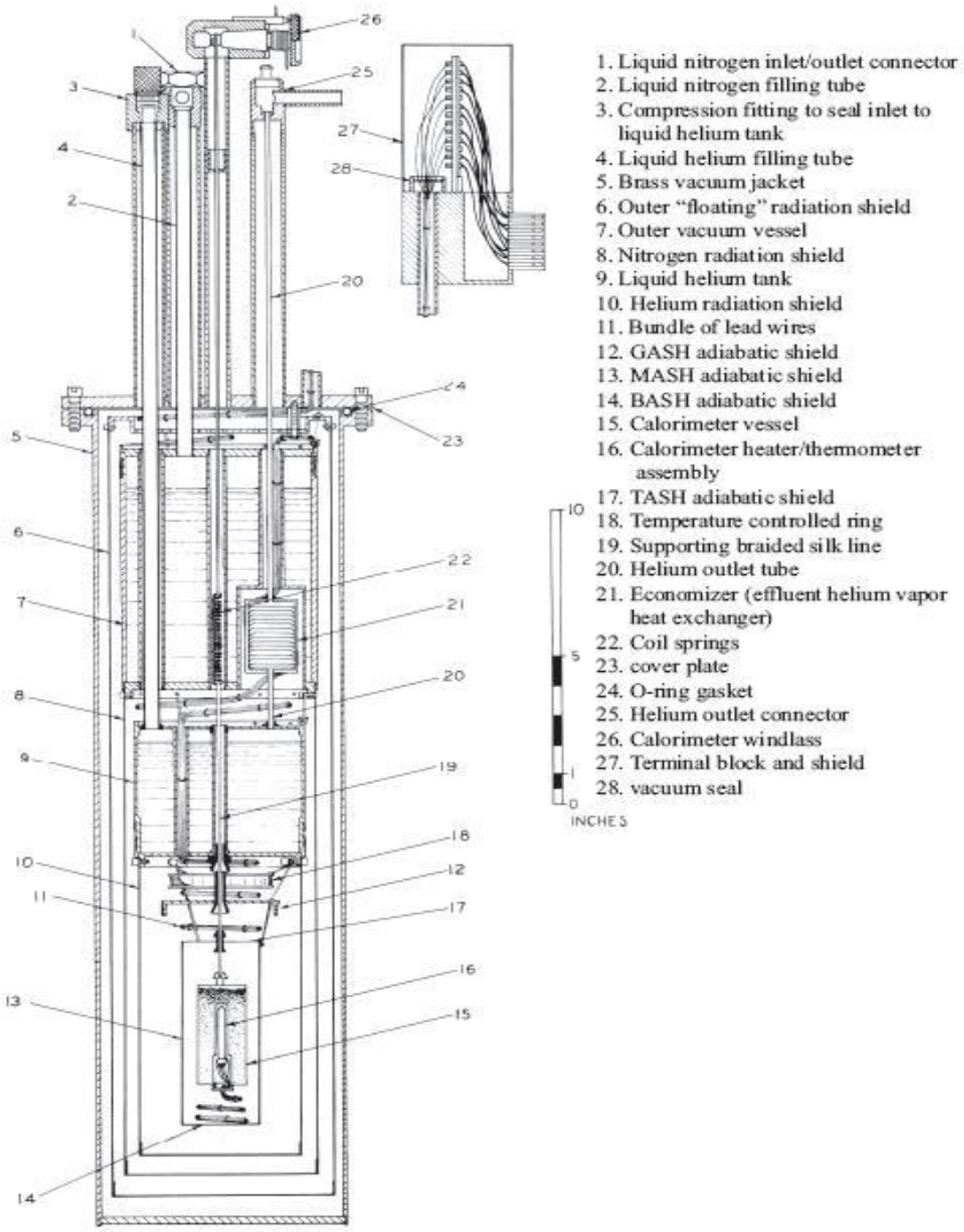

Figure 3.2: Large-scale calorimeter cryostat[1]

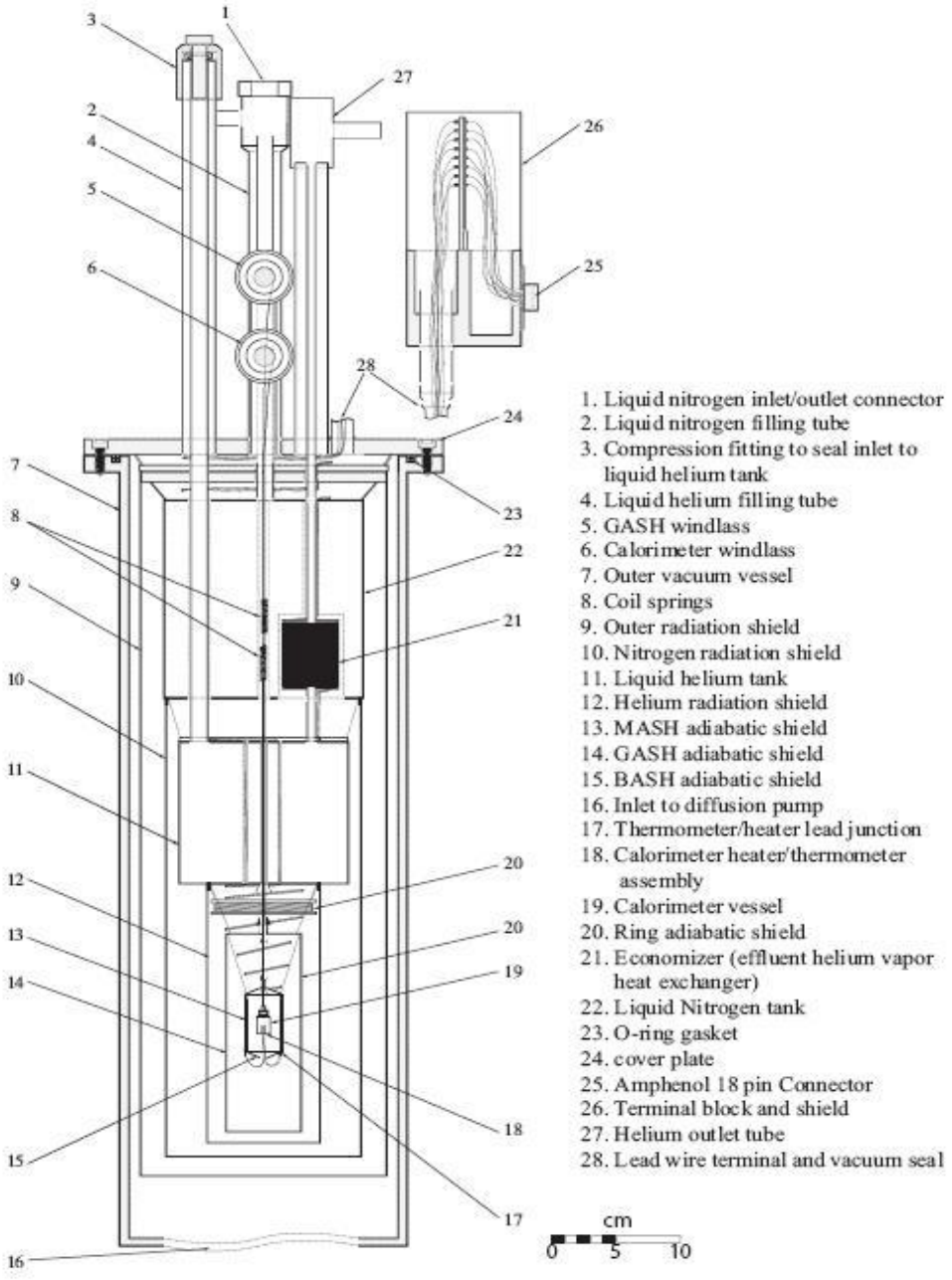

Figure 3.3: Microcalorimeter cryostat[1]

The design of the calorimeter vessel itself is, except for the size, the same for both instruments. The large-sample calorimeter has a 10.5 cm^3 internal volume. The calorimeter in the small-sample unit has an internal volume of 0.875 cm^3. A thermometer well is located in the bottom of the calorimeter; Apiezon T grease is used to provide thermal contact between the thermometer/heater and the calorimeter. A nut and cone, with a gold gasket to seal against the knife edge, allow the calorimeter to be loaded, evacuated, then back-filled with helium gas for thermal contact and then sealed. Wells on the side of the calorimeter vessel keep thermocouples in contact with the calorimeter; these also contain small amounts of Apiezon T grease to improve thermal conductivity. These thermocouples provide the primary electronic signals to control the adiabatic shield temperatures to track that of the calorimeter (Figure 3.4).

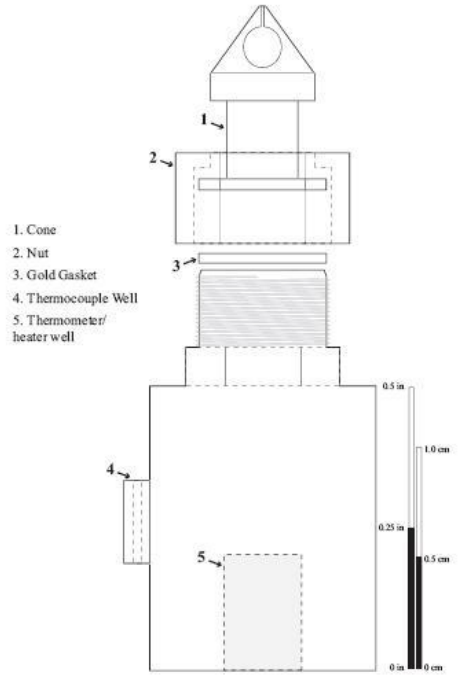

Figure 3.4: Microcalorimeter vessel[1]

3.1.3 Adiabatic Shields

Heat leaks into or out of the calorimeter are minimized by controlling the temperature of the environment immediately surrounding the calorimeter, using adiabatic shields (see Figure 3.3). The design of the calorimeter is such that the sample temperature and the amount of energy put into the calorimeter are measured and controlled as accurately and reproducibly as possible. The adiabatic shields are equipped with thermocouples (TCs) and heaters. The thermocouples transmit voltages proportional to the temperature differences between pairs of control points to the computer that provides PID control (explained further below) for the shields, and the computer then controls the heater voltages applied to the shield to minimize the shield-calorimeter temperature difference.

In the microcalorimeter cryostat, there are five adiabatic shields; in the large cryostat there are four. These five are labeled MASH, the middle adiabatic shield heater, TASH, the top adiabatic shield

heater, BASH, the bottom adiabatic shield heater, RING, a ring-shaped heater around which are wrapped wires that lead to and come from the calorimeter and shields, and GASH, the guard adiabatic shield heater. The first four shields are found on the large calorimeter; GASH is unique to this cryostat and not found on the large cryostat.

MASH, a cylindrical shield, surrounds the calorimeter. It is the second-largest of the shield heaters. TASH is the top end cap on MASH, and it is tightly fit to MASH. BASH can drop down from MASH for unloading, but it is connected to both MASH and the rest of the cryostat by wires from the rig to the shields and the thermometer/heater assembly. RING is supported over the MASH/BASH/TASH assembly. GASH, similar in shape to MASH but much larger, is unusual in that it is the only one of the shield heaters that is completely removable from the rig, as it encloses the entire MASH/BASH/TASH assembly and must be removed for loading and unloading.

The TCs on the shields all eventually connect to military-grade pin connectors at the top of the cryostat that are connected to the shield control computers and the power supply and voltmeters for the shields. GASH, being removable, also has connectors on its outside surface to connect the heaters and TCs to the instruments when loading.

The computer PID control is thoroughly explained in Brian Lang's dissertation, but a short explanation of the basic principles will benefit this discussion. The computer controls the shields using a feedback algorithm. Each TC returns a voltage that is proportional to the temperature difference between the surfaces where the TC junctions are fixed. The computer receives this voltage from each TC, and compares it to the setpoint of the particular shield in question. That means the PID control computer compares the TC reading on a particular shield to its zero point, i.e. for MASH, the zero point is at the temperature of the calorimeter; for RING, it is at the temperature of MASH, and for GASH, it is at a point offset ostensibly colder (by 0.01 mV) than the TC voltage of MASH. The shield heater power supplies alter their output to increase/decrease heating based on the setpoint comparison, thus changing the reading. This causes the computer to again direct a response or not, depending on the magnitude and direction of the new reading change.

3.1.4 Shield Control

Each shield is connected to a voltmeter to receive the input from the TCs. These voltmeters then communicate with the PID computer. These voltmeters can set a voltage offset for each shield, depending on how heat flow is expected or is observed to behave. Permanent offsets are applied to GASH and RING, while the offset for MASH is adjusted to obtain optimal temperature control. As data is collected, the general drift of the data is observed. The drift refers to the measuring of the temperature of the calorimeter and sample over a period of time with, ideally, no heat entering or leaving the sample. However, there tends to be cooling or heating in the drifts, mainly from heat flowing between MASH and the calorimeter, hence the MASH offset. If the calorimeter temperature is drifting to colder temperatures, the offset is changed to a more positive voltage, i.e. warmer, as heat is being lost by the sample, so the shield offset compensates. If the opposite case occurs, i.e. that the temperature is becoming warmer, then the shield is set to a more negative voltage, i.e. a colder offset. These changes are made in the middle of a pulse in data collection to allow the change to be averaged over the pulse.

These voltmeters and the control computer receive measurements from the TCs. The TCs are not configured to report absolute temperatures; instead, temperature differences reported relative to a control point are measured. In this case, the MASH thermocouple, connected to TCs on its inner surface and TCs inserted in the wells on the calorimeter vessel body, reports to the voltmeter and the computer the temperature difference between MASH and the control point on the calorimeter. Deflections of the voltmeter needle indicate the directionality of the temperature difference. The needle moves one way if MASH is colder than the sample, and the opposite direction if it is warmer. RING's TC measures the temperature of RING relative to MASH, as does GASH's TC. In Lang's early studies,[1] it was shown that individually controlling the BASH and TASH heaters disrupted the MASH control. Therefore their outputs were connected in series to that of the MASH power supply. This results in the information from the MASH TC being used to control MASH, BASH, and TASH as one unit. Though TASH and BASH TCs are extant, they are not used.

TC input from the shields drives the PID control process. This input is given to the PID computer through the IEEE-488 interfaces on the voltmeters, and the computer then adjusts the amount of power to the shield heaters through their power supplies. These power supplies, usually controlled entirely by the

PID computer running a LabView interface, have an analog display of the percentage of current being applied to the shield heater, as well as a digital display of the setting for the current. The PID interface on the computer control has two extra settings, for 300mA and 400 mA, for the maximum current setting. The actual power supply does not have these settings, so the digital display reads 500 when any of the 300, 400, or 500 mA settings are chosen.

Control of the GASH shield heater differs slightly from the other shields. As it is the largest of the shield heaters, the concern existed that heat could flow to the calorimeter,[1] so the shield heater is set at an offset of 0.01 mV to keep it permanently cold with respect to the calorimeter. This permanent offset facilitates control of MASH by providing a small amount of cooling power while maintaining a constant ΔT. This prevents having to change the MASH shield settings drastically. To a smaller extent, the RING heater is also offset cold with respect to the sample.

3.1.5 Position Control by Windlass

When loading the calorimeter into the cryostat to begin measurements, the calorimeter is hung on a string and pulled up into the MASH assembly. Specific positions of the calorimeter relative to the interior of the cryostat are noted by reading off the numbers on the dials on the windlasses. One windlass allows separate raising of the GASH assembly, while the other controls the calorimeter and the MASH assembly, and can raise the GASH assembly if necessary, but this is usually avoided to prevent stress on the string. Important positions include the data collection position, where the calorimeter is approximately in the middle of MASH, used when data is collected; the TASH position, where the calorimeter is just barely in contact with TASH; the GASH position, where the TASH/MASH/BASH assembly is in contact with GASH; and the full cool position, where the GASH assembly is in contact with the helium tank and cooling is most rapid.

3.1.6 Calorimeter Wiring

The wires for shield heaters, shield TCs, and the thermometer/heater leads connect to the data collection and PID control computers via three connectors at the top of the cryostat. The cables to the

computers and the other instruments are disconnected at this point when unloading the sample. Upon loading, the wire continuity is tested at these connectors as the easiest contact point.

3.1.7 GASH Wiring

The wires connecting GASH to the cryostat are unique in that they are handled every time the calorimeter is loaded and unloaded. These wires connect the GASH heater and the GASH TC to the rest of the instrument. They are either varnished to the top of GASH, i.e. the place where the GASH shield is screwed in place upon loading, or they hang from elsewhere on the rig body. When connecting the wires to GASH, they are physically manipulated with tweezers to seat the pins to their connectors. These wires have more free-hanging length than other wires, in order to allow easier handling. Most other wires are varnished or held in place as much as possible to minimize movement, as movement increases stress on the wires. The GASH connections are made through the use of male and female pins soldered to the ends of the wires from the cryostat and the wires on the GASH shield. The GASH pins are varnished in place to allow the easy movement of the wires from the cryostat for connection upon loading.

This repeated handling has led to the need to repair to the GASH wires. On one occasion, one wire broke and had to be repaired by attaching an extending piece of wire to the wire from the cryostat, soldering it, and then covering that joint with heat shrink tubing. The pin was then soldered to the end of the extension. A common repair is to simply revarnish the pin connections on GASH, as handling can loosen them.

3.1.8 BASH Wiring

The wiring around BASH is significant because of its effect on loading the cryostat. The wires that connect BASH to MASH and the electronics (data collection computer, PID control computer, etc.) are a bundle that runs from the connection of the thermometer/heater leads, up to MASH, and from there to the electronic controls for the cryostat. During unloading, the BASH shield is removed from the bottom of MASH to allow the calorimeter to be lowered for removal of the TCs from the wells on the side of the calorimeter vessel. However, care must be taken because the bundled wires are essentially the only

connection between BASH and MASH when it is opened. This means that when BASH is open, it can hang from that wiring, thereby stressing those wires. Care is taken to minimize the time BASH hangs from the wires; a small wire hook holds BASH when no work is being done with the calorimeter or the MASH assembly. It is possible to remove the TCs from the wells while BASH is on this hook, however, the space available to work with the calorimeter hanging on the thread is limited and care must be taken to avoid damaging the calorimeter and stressing the wires.

These wires, bundled as the direct connection from the thermometer/heater leads to the electronics, are joined by the BASH heater and thermocouple wires. The BASH heater is simply a resistive wire coiled on the bottom of MASH, then covered with varnish for insulation and to hold it in place. The wires to and from the thermometer/heater are also kept insulated and separate from the BASH heater, as they run from the connection to the thermometer/heater to MASH.

3.1.9 Thermometer/Heater connection, Leads to Wires

The design of the calorimeter places the thermometer/heater leads hanging out from the bottom of the vessel (see Figure 3.5). These 0.005 in. diameter phosphor bronze wires are soldered to the wires to the electronics when loading, and unsoldered when unloading. For reference, the portions of the wires from the thermometer/heater to the connection will be referred to as leads, and the wires from the connection to the instrument, also 0.005 in., will be referred to as wires. The thermometer/heater assembly is vulnerable to heat flow through its wires; seemingly small changes in the position or wiring of the assembly can cause contact with the shield heaters, producing a heat leak that can change the measurements significantly.

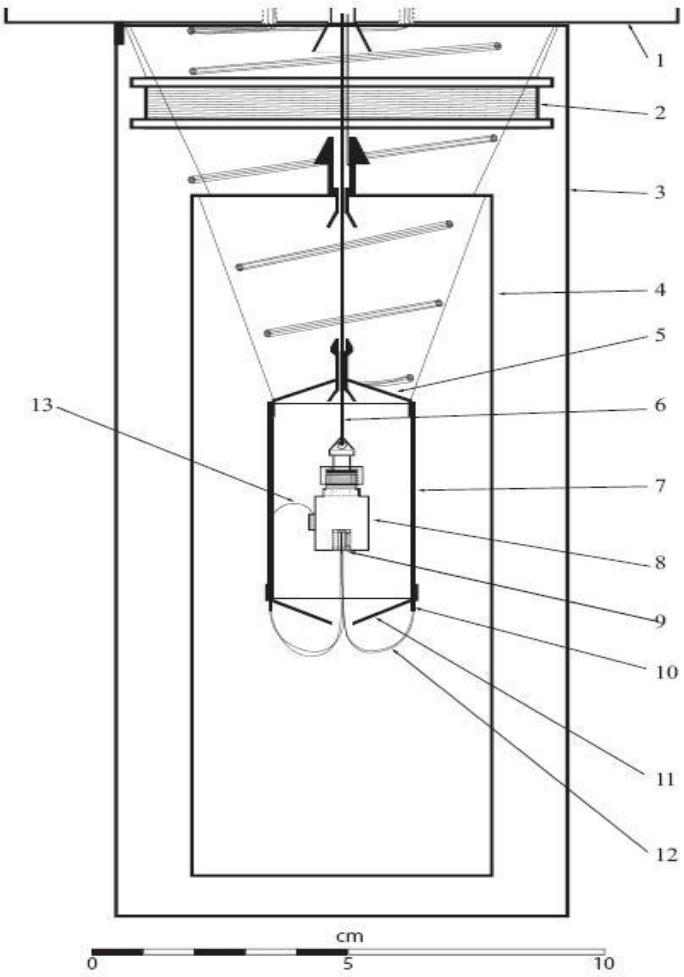

1. Bottom of liquid helium tank.
2. Ring adiabatic shield
3. Helium radiation shield
4. GASH adiabatic shield
5. TASH
6. Silk thread for suspending the calorimeter
7. MASH adiabatic shield
8. Calorimeter vessel
9. Calorimeter heater/thermometer assembly
10. Thermometer/heater lead junction
11. BASH adiabatic shield
12. Thermometer/heater leads
13. MASH thermocouple leads

Figure 3.5: Closeup of original thermometer/heater lead arrangement[1]

The BASH shield heater holds the connections for the thermometer/heater leads to the electronics. As described by Brian Lang,[1] BASH was constructed with a hole in the middle. The leads from the thermometer are passed through this hole while loading, being careful to neither pull the assembly from the well, nor snag the other wires inside or outside the TASH/MASH/BASH assembly. This has the effect of helping to center the calorimeter vessel inside the T/M/B assembly. In order to improve the centering, the

connections for each of the seven leads from the thermometer/heater were spread evenly around the bottom surface of MASH.

The thermometer/heater leads were connected to the wires from the electronics by varnishing the wires from the electronics onto BASH, keeping them thermally insulated from BASH with varnish underneath them. Metal, L-shaped posts were soldered to these wires, with the free leg of the L perpendicular to the surface of BASH. These solder joints were covered with varnished filter paper to assist in holding the joints together and to BASH. On several occasions, however, these posts came loose, so the filter paper also helped to allow reconnection of the posts to the wires in the extant solder joint.

When these posts come loose, the procedure is to heat the solder, typically present in a "ball" or "mound" of large enough size to allow manipulation without risking the wire coming loose, and reinsert the post and allow cooling. At times, this procedure requires removing the filter paper to allow better contact with the solder joint. The post would then be reinserted, and new filter paper is varnished over it.

For connecting the thermometer/heater leads to the posts on BASH, the calorimeter is hung on the string and raised enough for the vessel to be out of the way, but have slack in the leads to allow manipulation. Each lead is pulled through the hole in the center of BASH. Once they are all through, BASH is closed and screwed onto MASH. The leads are carefully arranged and pulled through to prevent snags, strain, or any interference with their play.

Brian Lang describes the arrangement and connection of the wires. Each of the seven leads from the thermometer/heater is soldered to a female connector pin. A stripped portion of each lead is inserted into a hole in the side of the body of the pin and through a matching hole on the other side. This lead then curls around the pin, and solder holds the wire to the pin. The main portion of the lead is arranged parallel to the pin and heat shrink tubing covers it. The female end of the pin is filled with solder. Each of these pins was customized from integrated circuit holders for circuit boards. Each lead is also labeled with some wrap on the wire insulation, using various colors for differentiation.

Each pin is carefully handled to prevent jerking and straining or breaking the lead. Tweezers are used to manipulate the pins. Each pin is heated by contact with the soldering iron to the end of the pin, and when the solder liquefied, the pin is quickly placed onto the post on BASH and let cool. Several difficulties exist with this process. First, heating the pin could loosen its connection to the lead, and the pin

would come off. This would have to be resoldered, generally not too time-consuming a process, but still tricky to avoid breaking the lead. Second, the pin needs to be firmly seated on the post, for stability and to produce a good, constant connection. Sometimes the solder would solidify before the pin had been placed as far as possible onto the post. The pin had to be reheated and either removed, or carefully moved to a more stable position farther on the post. Finally, the posts on BASH sometimes loosen or come off as a result of too much heat from the soldering iron. They need to be checked and replaced.

3.2 Attempting Repair of the Connection posts

The need to replace the posts occurred with increasing frequency after multiple calorimeter loadings. At one point, one of these posts came completely off. The post itself separated from the solder and the wire that connected to the rest of the instrument. The remedy seemed to be simple: resolder the wire to the post.

3.2.1 Attempts to Repair

As previously described, the connection between the post and the wire was a delicate and carefully set arrangement. The end of the wire and the post were connected only by being inside the "mound" of solder, which was then covered with filter paper varnished in place. Optimally, the wire and the post should be physically held together, by wrapping the uninsulated end of the wire around the post. The small amount of wire available, and the small amount of space available prevented this from being feasible. These connections served well enough to reproducibly conduct the current from the power supply through the thermometer/heater. The wire itself was wound around BASH and varnished to the surface. However, the solder "mound" itself only made contact with the wire and the post; it had no adhesion to BASH, hence the filter paper was needed to help hold it to the surface. This tenuous connection held over time, but required a delicate balance in maintaining the solder as the joint between post and wire.

When the post came loose from the solder, attempts were made to replace it. Heating the solder and inserting the post, then letting it cool was the first attempt. This, however, did not work. Next, we exposed the wire on BASH and attempted to remake the connection with the wire, the solder, and the post. This also did not work. Repeated attempts over time only caused the wire to break and more had to be exposed.

When the wire varnished to BASH broke, more had to be unvarnished from BASH. This, as well as strain from manipulating the wire and the post, and the proximity of the soldering iron to both BASH and the MASH assembly caused concern about continuing this avenue of repair. Heat from the soldering iron could affect other solder joints, and perhaps ignite flammable varnish or other materials.

After repeated attempts, a suitable and stable connection could not be made in this position. For continued, repeated operation, the post needed to be stable enough that attaching a heated pin with liquid solder would not break the connection with the wire. Past history and current attempts showed little possibility of a repair in the current arrangement. At this point, repairing the post was deemed unfeasible.

Previously, plans had been made to change the arrangement of the thermometer/heater wires. Having the wires outside the MASH assembly exposed them to the vacuum instead of keeping them close to the shield heaters. This led to a heat leak from the wires that had to be compensated for in the data collection program. The plan had been to connect the wires to pins on a semicircle connector installed on the inside of BASH and insulated from BASH. The connector had been installed already on the inside of BASH, prior to my work, but no connections were made to it at the time I began the repairs.

3.3 Redesigning the Wire Connections

3.3.1 Physical Arrangement

The setup of the wires, BASH, and the calorimeter complicated the rearrangement of the connections. Space inside the MASH assembly where the wires could be placed was limited; previously they hung relatively freely outside and had room to avoid contact with GASH (Figure 3.5, above). In order

to create the reproducible conditions necessary for measurements, the wires to the cryostat and the heater/thermometer assembly needed stable, sturdy connections. These connections needed enough flexibility to allow the opening and closing of BASH for loading and unloading. The arrangement also had to prevent physical, thermal, and electronic interference between various elements of the assembly.

The placement of the connector on the inside surface of BASH is fairly simple (Figure 3.6). BASH itself has some concavity, with the hole in the middle essentially the center of the concavity. The connector is arranged with the thermocouple wells facing the center of the open side of the semicircle, and the hole in BASH at the center of the semicircle. The BASH thermocouple, whose input is not actually used, (see description of MASH/TASH/BASH arrangement above) is short enough that when the thermocouple is in the well, it holds BASH slightly higher than normal, i.e. the shortness of the thermocouple wires reduces the distance BASH can hang down. The wires to the cryostat, which mainly support BASH if BASH is left free-hanging, are also towards the open side of the semicircle of the connector, i.e. that side of BASH is where they transfer from BASH to the MASH assembly.

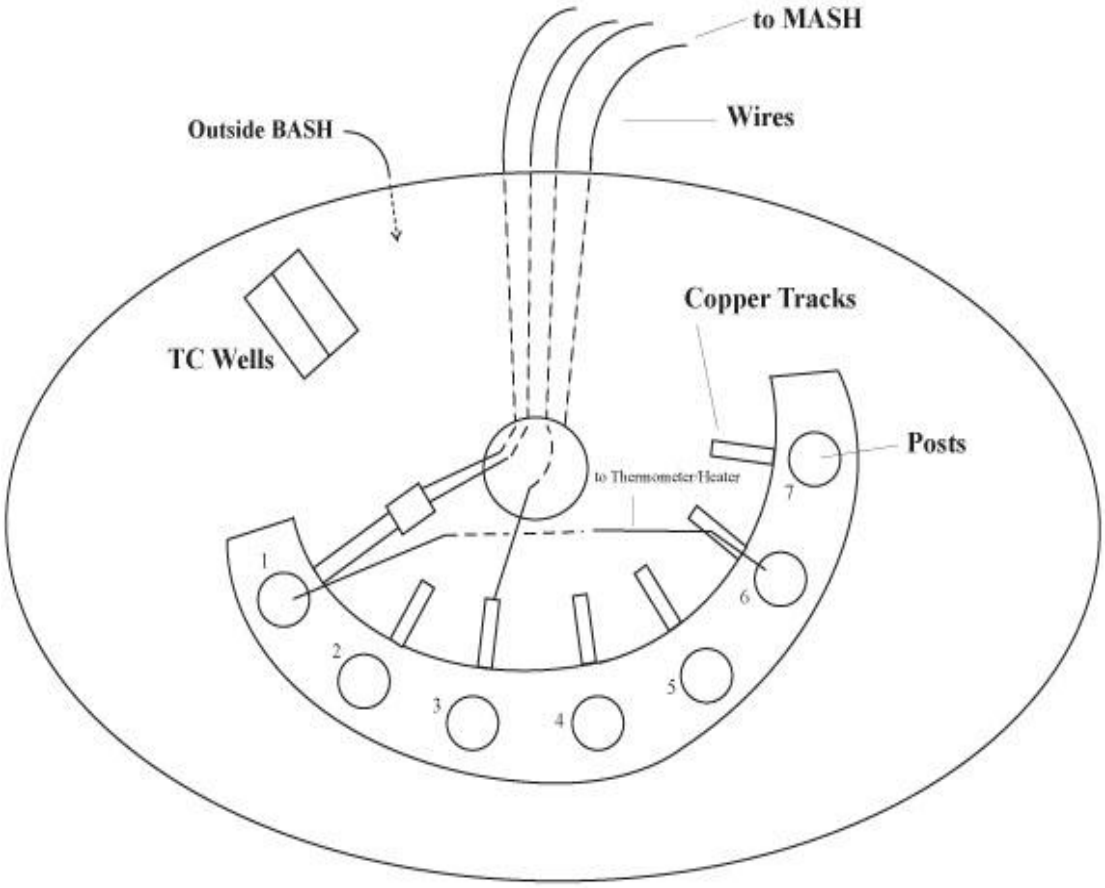

Figure 3.6: Diagram of BASH with new arrangement

The connector itself is an insulated platform, with seven posts out the top. Each post corresponds to a small hook on the side of the connector, facing inward towards the middle of the semicircle and the middle of BASH. These posts are sufficiently long that the pins could be reasonably soldered on them and expected to hold. The connector is sufficiently offset that it does not risk coming into contact with the side of BASH nor the side of MASH, when closed.

3.3.2 Moving the Wires

The change in location of the thermometer/heater lead connection to the cryostat required that the wires to the cryostat be brought inside BASH through the hole in the bottom of BASH. This change created two problems: first, some of the wires were too short to make the connection; second, actually making the connection of the wires was difficult to do, due to space and limitations of the solder. Extending the wires solved the first problem. This involved taking another section of the same type of

wire, and soldering it to the end of the wire to be extended, hooking exposed ends together for greater strength. Heat shrink tubing covered this for insulation and extra support. During manipulation of these wires, several broke so that they also had to be extended.

The solution to the second problem was more involved. The hook intended for the connection of the wires is very small, and difficult to even touch with the soldering iron. The area in the center of BASH, surrounded by the connector and the thermocouple wells, limits the access to those hooks and the wires. Maneuvering the very small wires required a dexterity and capability not possible in the small space available. The solder also would not stick to these hooks, preventing connection.

An alternate solution allowed stable connections of the wires to the posts. Small, rectangular copper strips, or tracks (Figure 3.6), with two holes provided contact for the wires to the posts. The wire was soldered into one hole, and then the other hole was lowered over the post on the connector as close to the base of the post as possible. The strip was then soldered to the post. These strips were made as short as possible while allowing connection between post and wire in order to prevent shorts between posts or to BASH.

One complication in moving the wires to the connector inside BASH involved the heater voltage and current wires. The two V^- and I^- heater wires coming from the top of the cryostat are connected at the same post to a single lead from the thermometer/heater assembly.[1] The bundle from the cryostat was too short to make the connection with the short strip, and bringing two wires together to one strip meant extensions were not feasible. The solution was to use a much longer strip of copper, carefully arranged with the wires soldered into the hole on the end of the strip like the others. This longer strip was also located to avoid shorts.

The wires themselves were rearranged to avoid stress and thermal and other interference. The wires were carefully bundled and tied off with silk thread on the inside of BASH. On the outside, they were carefully varnished to the BASH surface. However, shortening this shortened the wires between BASH and MASH, lessening the "slack" in the wires available to manipulate BASH when loading and unloading. The space available to manipulate the calorimeter within MASH was thus reduced. This also required allowing BASH to hang from the wires in order to solder the leads to the posts.

3.3.3 Rearranging the Thermometer/Heater Leads

Previously, during the loading procedure, the thermometer/heater leads would be fed through the hole in BASH and then soldered to the posts outside BASH. With BASH screwed firmly in place to the MASH assembly. After moving the wires, the pins needed to be soldered to the pins on the connector with BASH open and hanging freely. This increased the difficulty of soldering. Care must be taken to minimize stress, i.e. too much strenuous motion on the BASH wires supporting the BASH assembly. Steady soft motion where necessary, supporting BASH as much as possible, and limiting the amount of time BASH has to hang freely minimize the stress on the wires.

The leads with the pins being moved inside needed to be arranged and organized for repeated loading (Figure 3.6). Each pin and its lead was carefully separated and arranged according to the chosen order. The pins were carefully heated and positioned on the posts on the connector. This was complicated both by the need to avoid heating the copper strips and by the difficulty of placing the pins firmly on the posts in the limited space and with the hanging BASH. The arrangement of the space inside BASH and below MASH suggests that the easiest method of soldering is to solder the rightmost post first, labeled 7 on

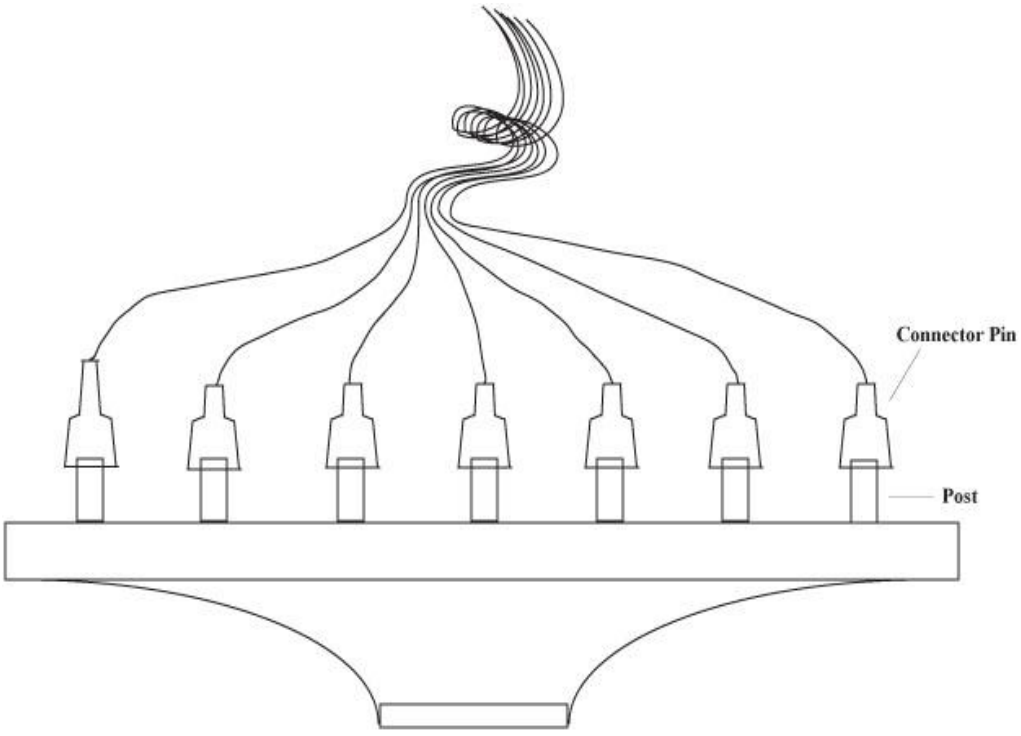

Figure 3.7: Side view of connection with pins on leads

the diagram. Upon completion, the continuity of the wires was checked to determine if the connection was properly made. If not, then the pin and the copper strip were checked and adjusted until a continuous connection was made.

When a good connection was established, the calorimeter was raised and the wires placed inside MASH. Care was taken in arranging those wires and the TC wires for the thermocouples placed in the TC wells on the microcalorimeter (Figure 3.7). The BASH assembly was then raised into place and screwed into place. This meant that the leads and the connections with the posts and pins were enclosed into the space inside MASH between BASH and the calorimeter.

3.4 Experiments with Benzoic Acid: A Test of Reproducibility

As previously indicated, experiments with benzoic acid were conducted to determine the accuracy and precision of the microcalorimeter compared to previously measured data. Pellets with mass of 0.525 g of benzoic acid were loaded into the calorimeter at an atmospheric pressure of 637.9 mm Hg, 52 % humidity, and a temperature of 23.21°C. The mass of the gold gasket involved in sealing the microcalorimeter was 254.53 mg, and the microcalorimeter was sealed with 11 mm Hg of helium gas after evacuating the calorimeter. Benzoic acid is a calorimetric standard provided by NIST. The literature reference data used here for comparison was from a sample run on the large calorimeter. That data had been collected and functions fit to the data, and those functions had been used to generate data for comparison on a previous run of benzoic acid standard on the microcalorimeter.[1]

3.4.1 Symptoms

Figure 3.8 shows that the data from several series of measurements, each individual series represented by different symbols, was not reproducible. Considerable scatter was seen in the data at high temperatures, and the data of a given series was higher or lower than a different series at the same temperature region. This was often much lower than the standard data. Although some noise in the shield

control was observed, the shields generally controlled well enough that this bad data, especially for so many series, could not be attributed to poor shield control. Another "symptom" of a problem was evident when the calorimeter was heated manually. Occasionally, for measurements at $T > 230$, the temperature reading when heating and not collecting data would spike randomly up and down, instead of the normal steady upward slope. Given the recent changes to the wiring configurations, investigation of the problem began with the physical arrangement of the instrument.

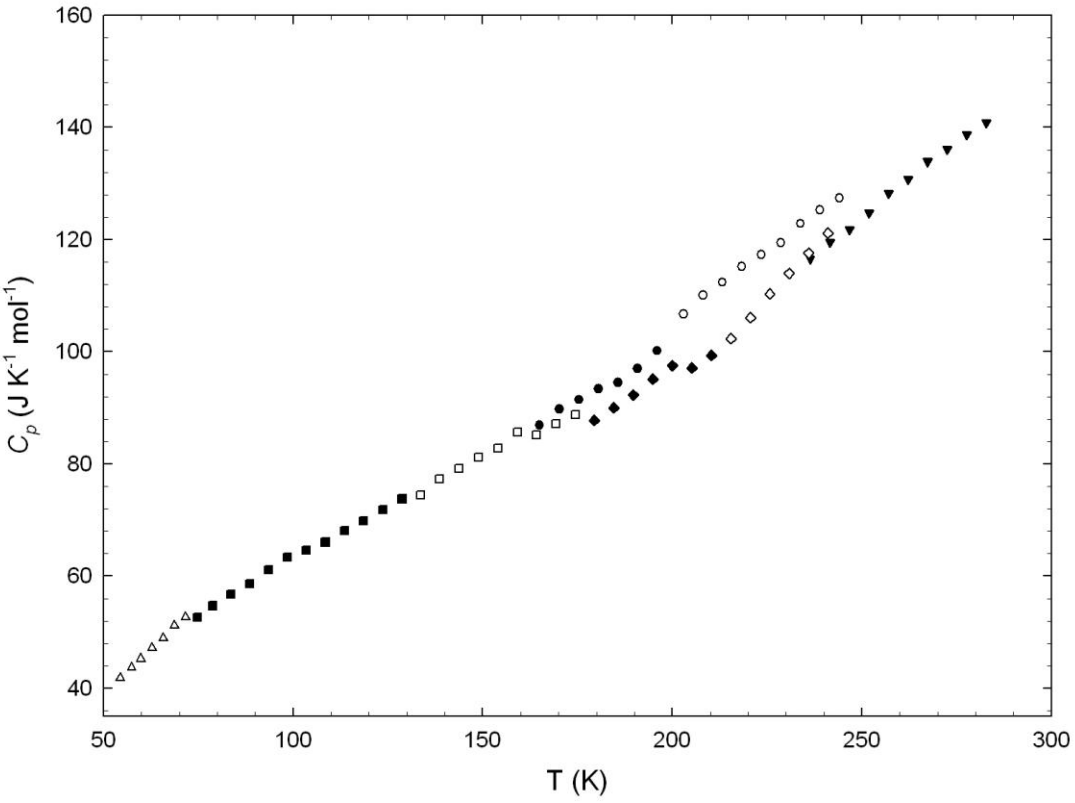

Figure 3.8: Initial benzoic acid specific heats. Different symbols represent different series of data.

3.4.2 Diagnosing the Problem

As a result of the previous arrangement of the lead wires, a correction for the heat lost from the wires hanging outside the MASH assembly was programmed into the data collection program. This correction was removed from the program, retained only as remarks in the program file, as a first attempt to

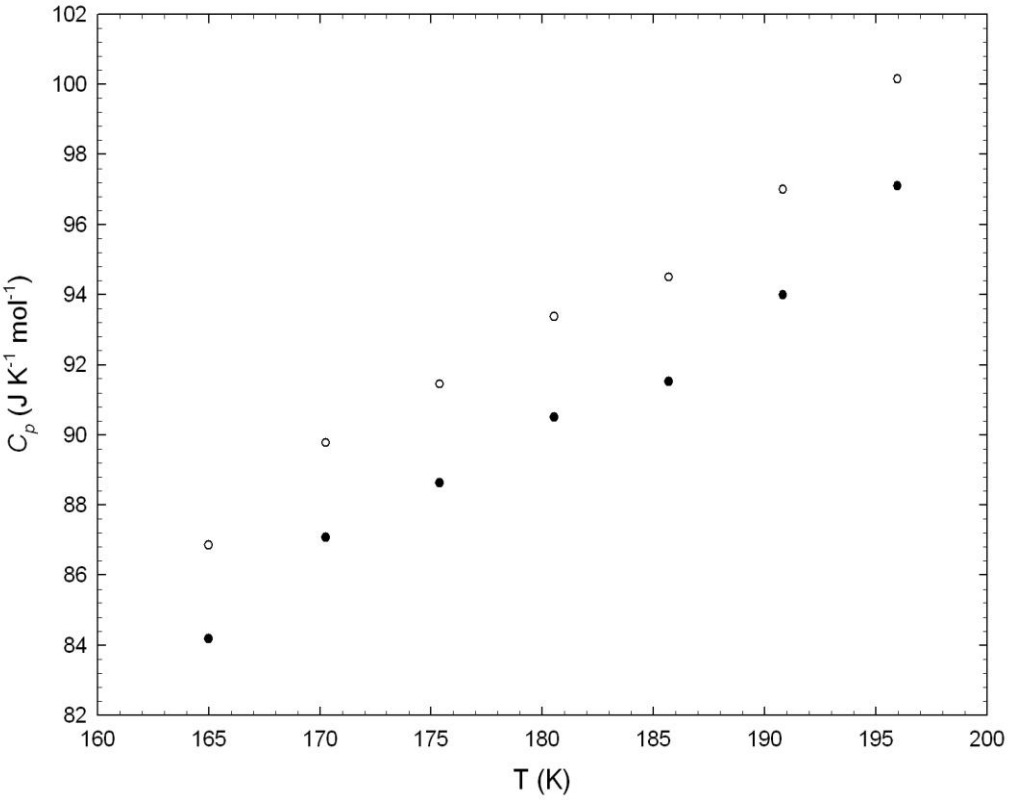

Figure 3.9: Benzoic acid with and without heat leak correction. Filled circles are with heat leak correction, open circles are without

find and correct the error. The hypothesis was that the correction might have been applied inconsistently when data with the different thermal behavior was collected. This was tested with one series of data, and found to have had only a small, constant effect on the reproducibility of the data(Figure 3.9). The data still was not reproducible.

The next concern was that heat was leaking out of the hole in the bottom of BASH via radiation. The suspicion was that this radiation leakage was random and not due to reproducible conditions. Previously, the wires hanging outside the MASH assembly radiated a measurable heat loss, accounted for by a correction in the data analysis software. Such irreproducible heat loss could cause the data to be inconsistent. This was tested by varnishing a small piece of common kitchen aluminum foil over the hole in the bottom of BASH. The wires leading into BASH to the thermometer/heater lead connector, with the heat-shrink-covered joints of the extended wires resting at the outside edge of the hole, anchored one side of the foil. Sufficient varnish covered any gaps between the foil, the wires, and anywhere where the foil could not be completely sealed against the surface of BASH. Once the varnish dried, the cryostat was reloaded. The cryostat was evacuated for longer than usual with the rough pump and the diffusion pump,

to allow any gases trapped in the new varnish to be pumped away. Several series of data showed that this also had little or no effect on the reproducibility of the data (Figure 3.10).

The next tests involved determining if BASH was interfering with the wires, causing heat flow into the thermometer from the heater. This required disconnecting BASH and TASH heaters from the MASH heater power supply. As stated previously, the two heaters were connected in series with the MASH heater to the power supply. This allowed the MASH thermocouple to control all three heaters.

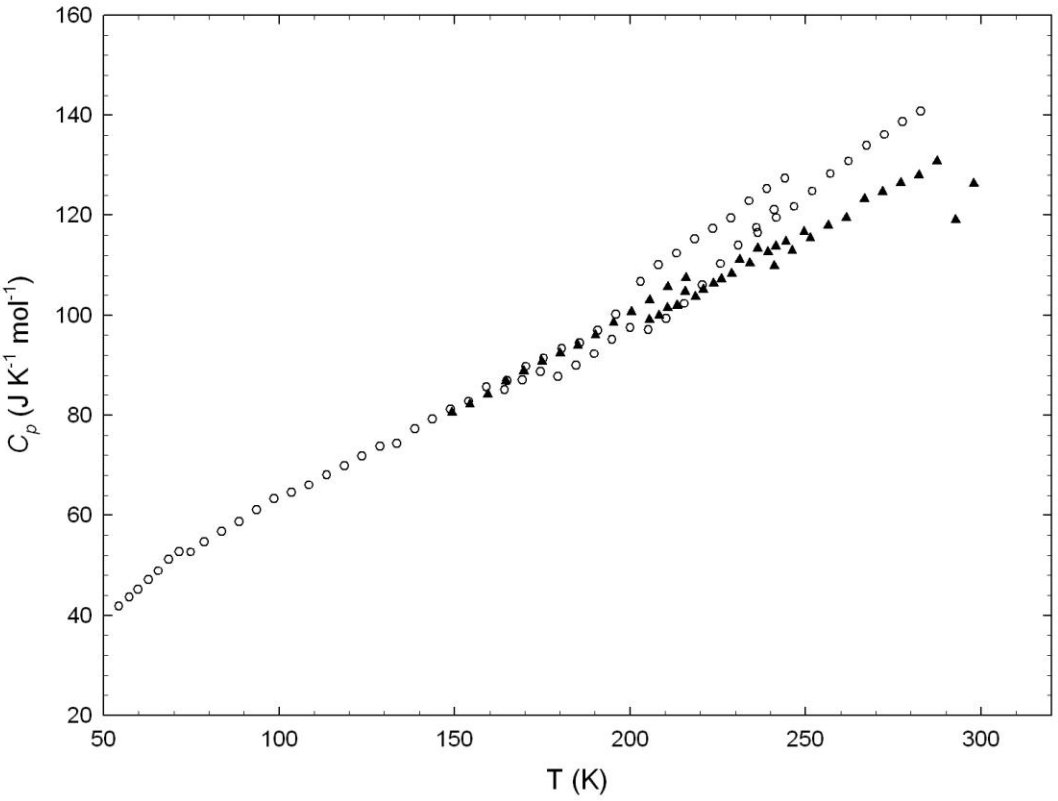

Figure 3.10: Benzoic acid after placing Al foil on BASH. Triangles are data after placing foil on BASH; open circles are data before foil.

Disconnecting the heaters allowed collecting data with BASH and/or TASH off or with constant current to see if the data was affected by these heaters. Data collected in circumstances with each heater off separately, together, and with constant current on each did not show improvements in the reproducibility (Figure 3.11). Figure 3.11 shows the data collected while testing the shield heaters. The data that is very far from the rest of the data, i.e. widely scattered below the general grouping of the other data, was

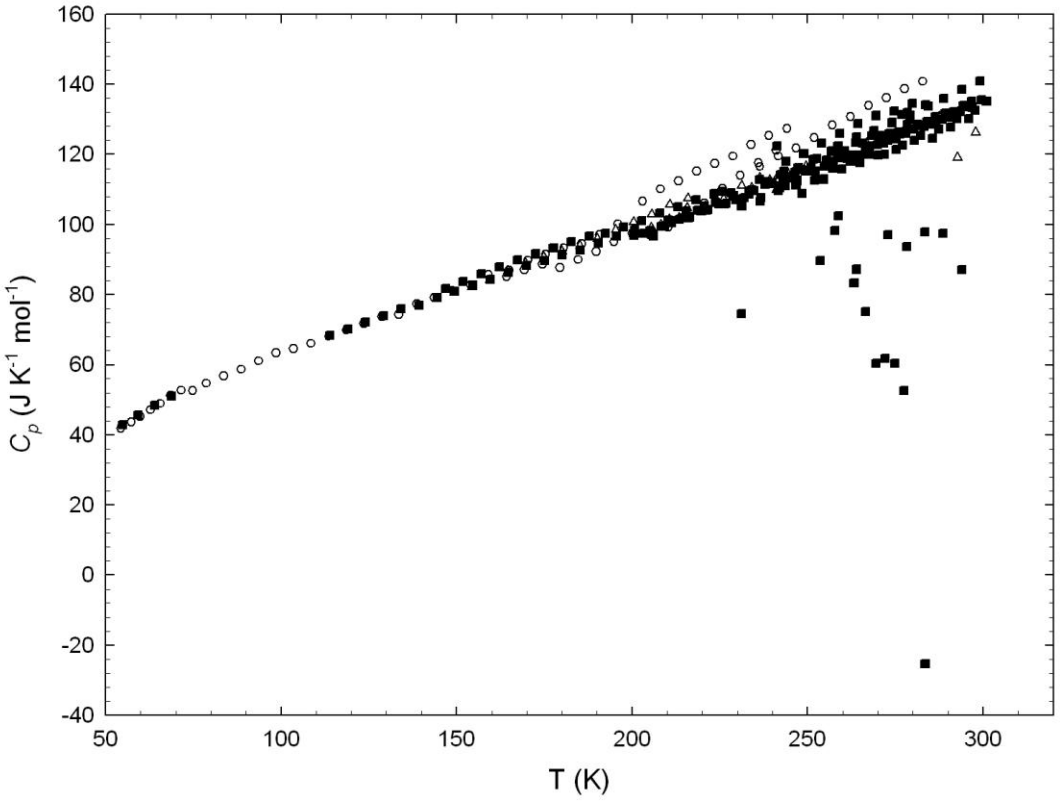

Figure 3.11: Benzoic acid after testing shield heaters

collected in runs 45-48, during the attempts to run with TASH off, on manual control, and with a constant current.

Data taken at low temperatures did not show the same scatter and inconsistency, although the accuracy was still suspect. The next series of data were taken with the offset on GASH set closer to zero than normal, and then with GASH turned off. Neither of these tests showed any improvement in reproducibility.

3.4.3 Leads Contacting MASH

Attempts were made to observe the effects of changing various elements of the system. One test involved turning off GASH and observing the effect on the temperature measurement as the GASH temperature drifted away from that of the calorimeter. It was observed that the calorimeter temperature began to increase significantly, at a rate between 20 and 30 mK per minute, where slight cooling or little to

no change would be expected. Over time, this led to great increase in temperature. Observation of the system during repeated tests determined that when GASH was turned off, MASH would heat to compensate for the cooling, and the calorimeter temperature would increase.

This observation led to the conclusion that the thermometer/heater leads were making contact with MASH, and heat was being fed directly into the calorimeter from MASH. This contact explained the irreproducibility and the noise. MASH heats or turns off according to input from the computer, as a response to changes in the TC reading. Heating of the calorimeter and therefore changes in the measured temperature occurred irreproducibly as a result of irreproducible changes in the MASH TC reading. This added differing amounts of heat at different times to the thermometer through wires contacting MASH. This also may explain the spikes when heating the sample, in that as the heater put energy into the calorimeter, over time, some of that heat would affect MASH, causing MASH to change its behavior and input energy into the thermometer by way of contact with the leads, possibly enough to interfere.

The arrangement of the leads became of concern upon discovery of the contact. By the previous arrangement, the leads were sufficiently long to allow feeding them through the hole in BASH and attaching them to the posts. This arrangement also had the benefit of helping to center the calorimeter as it hung. Now, however, the length of the leads required considerable space in order to accommodate them inside the MASH assembly. Also of concern were the pins, which forced the wires into a vertical position at the connector. This reduced the space available to the leads and restricted the ability to maneuver the leads away from the sides of MASH.

3.4.4 Adjusting the Lead Arrangement

Multiple attempts at rearranging the wires had mostly no success, although one set of data series appeared to show consistency. The leads were coiled as much as possible, and the excess leads bunched in the middle of BASH, in the hope of avoiding unwanted contact with MASH. The one seemingly good set of data occurred when as much of the excess leads as possible was pushed together down into the concavity in the middle of BASH, towards the hole in the middle. However, this result could not be repeated after again opening up the cryostat and raising and lowering the calorimeter to observe reproducibility from load

to load. It appeared the leads were too long, and not enough space was available for the wires to be consistently kept free from contact.

3.4.5 Shortening the Leads

Shortening the leads became the only option. Two contrasting needs were to keep the leads long enough to allow maneuvering and raising the calorimeter, and yet short enough to minimize risk of contact with MASH. Enough slack in the wires allows the calorimeter to be maneuvered on loading, the leads and the pins to be soldered to the posts with relative ease, and the calorimeter raised to contact with TASH for cooling. Another concern is keeping the calorimeter centered in the MASH assembly. The change in arrangement of the wires also changed their effect on the calorimeter's centering. Too much length increases the risk of contact. The leads were cut *in situ* to allow a practical determination of appropriate length based on the vertical and horizontal centering of the calorimeter.

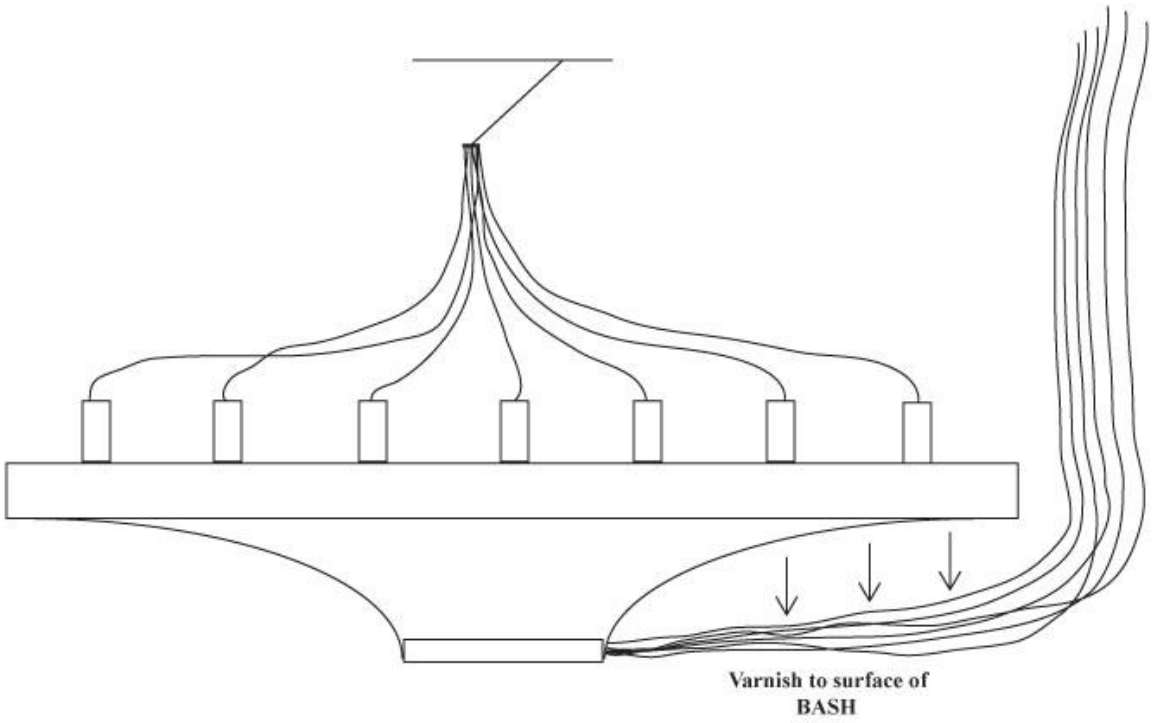

Figure 3.12: Side view of thermometer/heater connection without pins

The wires and pins were arranged to leave a significantly smaller loop of wires still in the middle of BASH. A portion of the leads from the thermometer/heater were coiled below the calorimeter in order to assist centering the calorimeter. The pins on the ends of the leads were removed to allow the wires to simply be soldered directly to the posts. The wires were arranged towards the center (Figure 3.12). Multiple series of data were taken to determine reproducibility. Irreproducibility in the measured data was noticed after opening the cryostat to simulate loading and unloading the calorimeter. The data before opening was consistent between series, but was higher than the data measured after the simulated reloading.

The arrangement of the wires and the centering of the calorimeter became the focus of the study (Figure 3.13). Repeated opening of the calorimeter and adjustment of the leads and centering of the calorimeter eventually led to relatively non-noisy data that was reproducible from series to series (Figure 3.14). The figure shows data over several series, including the region below 50 K, where liquid helium is needed to collect data. The cryostat was opened and the calorimeter lowered several more times to again simulate loading and unloading different samples, to determine consistency with repeated rearrangements of the wires. The data from 22 K to 50 K was then collected for the benzoic acid using liquid helium.

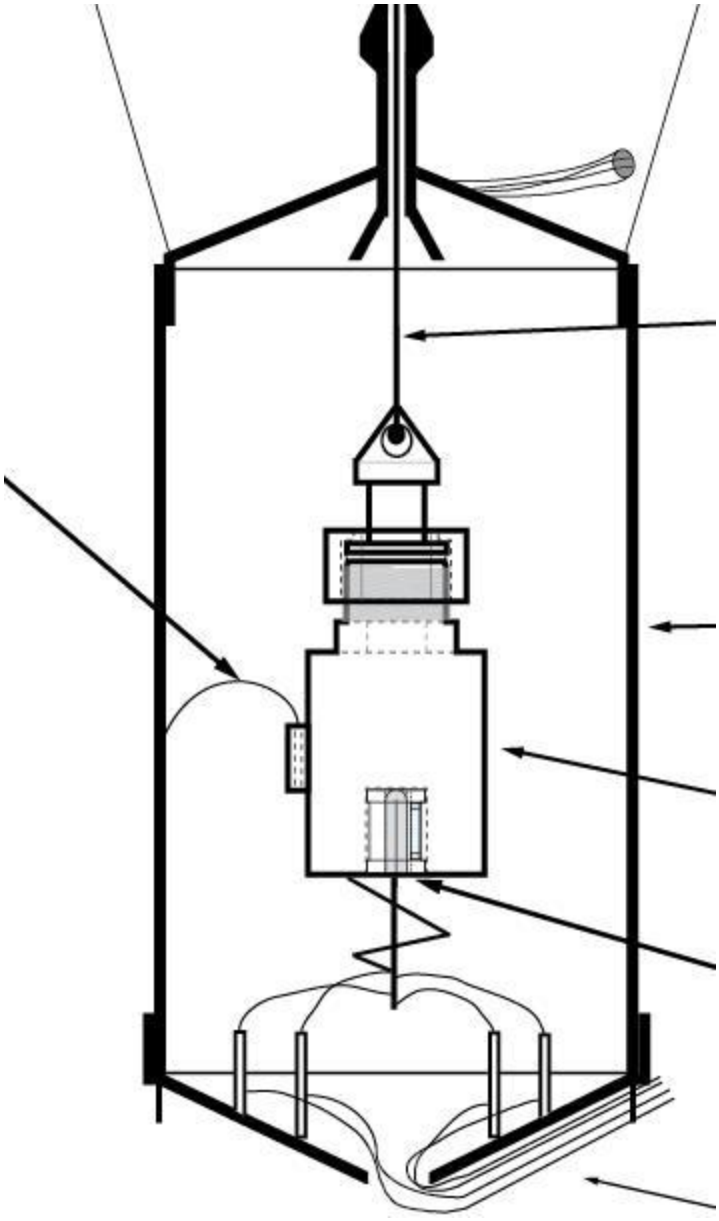

Figure 3.13: Microcalorimeter with new thermometer/heater lead arrangement

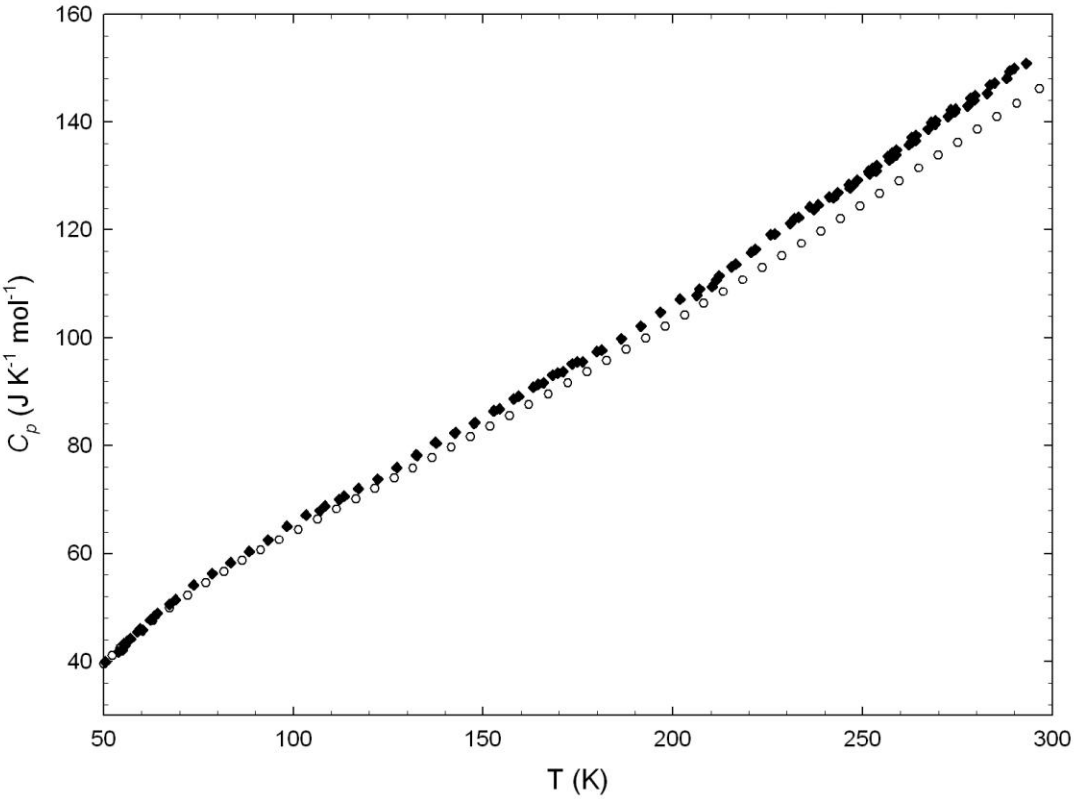

Figure 3.14: Benzoic acid final data. Diamonds are the experimental data; Circles are a benzoic acid standard.

3.4.6 Conclusions and Future Work

The completion of the data collection allowed the removal of the benzoic acid from the calorimeter, after having been in the calorimeter approximately 2 years. In order to get a complete understanding of the accuracy and precision of the instrument after the changes, a new empty has been run. The data from the benzoic acid is not consistent with the standard by about 2 percent at high temperatures after the new empty. The new empty shows that the changes had an influence on this difference, but other factors may also be involved. The difference suggests that the previous heat leak, thought to be eliminated by moving the wires inside the calorimeter, still exists. Another factor may be the condition of the sample observed after unloading. Green flakes were seen on and mixed among the white benzoic acid sample.

This suggests that some small error may originate from copper benzoate, a product of the acid reacting with copper from the calorimeter.

The current possibility of a heat leak is being investigated. The previous heat leak,[1] accounted for by Brian Lang in his dissertation, may still be a factor, and the assumption that moving the leads and wires inside the MASH and BASH assembly removed that leak may be wrong. It may also be another or new heat leak, possibly heat being transferred up the thread on which the calorimeter vessel hangs. Efforts are underway to determine both the source and an appropriate correction for this problem.

References

1. Lang, B. E.; Specific heat and thermodynamic properties of metallic systems : Instrumentation and analysis. Brigham Young Univ., Provo, UT, USA. Avail. UMI, Order No. DA3193054. (2005), 247 pp. From: Diss. Abstr. Int., B 2006, 66(10), 5423. Dissertation written in English. CAN 145:196721 AN 2006:771573 CAPLUS
2. Robie, R.A.; Hemingway, B.S.; Fisher, J.R.; Wilson, W.H.; Heat-capacities of Gibbsite, $Al(OH)_3$, between 13 and 480 K and Magnesite, $MGCO_3$, Between 13 and 380 K and their standard entropies at 289.15 K, and heat-capacities of Calorimetry Conference Benzoic-Acid between 12 and 316 K *J Research of the US Geological Survey,* **1977,** *5,* 797-806
3. Kaji, K.; Tochigi, K.; Misawa, Y.; Suzuki, T.; An adiabatic calorimeter for samples of mass less than 0.1 g and heat-capacity measurements on benzoic acid at temperatures from 19 K to 312 K *J Chem Thermodynamics* **1993,** *25,* 699-709
4. Stevens, R; Boerio-Goates, J; Heat capacity of copper on the ITS-90 temperature scale using adiabatic calorimetry. *J. Chem. Thermodynamics,* **2004,** *36,* 857-863